*drugs and drug candidates*

MDPI

*Article*

# Structural Insights into the Redox Potential of Curcumin Derivatives in *Litopenaeus vannamei*

**Damião Sampaio de Sousa [1,2], João Miguel Lopes de Melo Lima [3], Carminda Sandra Brito Salmito-Vanderley [2] and Emmanuel Silva Marinho [1,2,*]**

[1] Postgraduate Program in Natural Sciences, State University of Ceará, Fortaleza 60714-903, CE, Brazil; damiao.sampaio@aluno.uece.br
[2] Postgraduate Program in Veterinary Sciences, State University of Ceará, Fortaleza 60714-903, CE, Brazil; sandra.salmito@uece.br
[3] Faculty of Veterinary Medicine, State University of Ceará, Fortaleza 60714-903, CE, Brazil; joao.miguel@aluno.uece.br
* Correspondence: emmanuel.marinho@uece.br

## Abstract

**Background/Objectives**: Curcumin derivatives have attracted interest due to their redox-modulating properties and potential applications in aquatic organisms, yet their molecular interactions and environmental safety remain insufficiently characterized. This study aimed to evaluate the redox-related molecular behavior and ecotoxicological profile of curcumin derivatives, with emphasis on their interaction with glutathione S-transferase from *L. vannamei*. **Methods**: Molecular docking and molecular dynamics simulations were performed to assess binding stability and interaction patterns between the derivatives and *Lv*GSTmu. In parallel, computational predictions were used to estimate environmental persistence, bioaccumulation (BCF/BAF), and acute and chronic aquatic toxicity across multiple trophic levels. **Results**: Docking and dynamics analyses indicated stable ligand–protein interactions, particularly for CURNO, which showed favorable binding behavior without destabilizing the protein structure. Ecotoxicological predictions suggested low bioaccumulation potential and limited persistence for most derivatives, with CURH and CURNO showing higher sediment persistence. Toxicity responses varied by organism and exposure time but did not differ significantly among derivatives relative to curcumin. **Conclusions**: The derivatives retained redox-related molecular features while presenting an overall acceptable predicted environmental profile. CURNO emerged as a promising candidate, although its environmental behavior supports the need for further monitoring and experimental validation.

**Keywords:** antioxidant; computational insight; *Curcuma longa*



Academic Editor: Žiko B. Milanović

Received: 28 January 2026
Revised: 13 March 2026
Accepted: 17 March 2026
Published: 7 April 2026



## 1. Introduction

Viral infections in crustaceans, especially by the white spot syndrome virus (WSSV), are strongly associated with the generation of oxidative stress and the modulation of the immune response [1]. WSSV infection profoundly alters the composition of the intestinal microbiota and the production of its metabolites, a phenomenon often related to immune dysfunction and increased susceptibility to oxidative stress [2].

To counterbalance this redox imbalance, crustaceans activate endogenous antioxidant systems, among which enzymes of the glutathione *S*-transferase family, such as *Lv*GST from *L. vannamei* or *P. vannamei*, play a central role [3]. These enzymes facilitate the conjugation

of reactive metabolites with reduced glutathione, promoting cellular detoxification and protecting tissues from oxidative damage [4,5]. Thus, the activation of these endogenous antioxidant mechanisms is an essential strategy to mitigate the deleterious effects of WSSV and preserve cellular homeostasis during infection [6].

In parallel with the study of synthetic antivirals, naturally occurring compounds have proven to be promising sources for the discovery of new therapeutic agents against viral infections in aquatic organisms [7,8]. Among these, curcumin consists of a bioactive polyphenol isolated predominantly from the rhizomes of *Curcuma longa* L., a species widely used in traditional Asian medicine, which has prompted extensive research into its pharmacological and biochemical properties [9].

In the scientific context, curcumin (Figure 1) stands out for its broad spectrum of biological activities, including antioxidant, anti-inflammatory, antimicrobial, antineoplastic, and antiviral effects, which are mediated by multiple molecular mechanisms and cellular signaling pathways [10,11]. Due to these pleiotropic properties, curcumin has high translational potential for pharmacological and biotechnological applications, particularly in the development of therapeutic strategies based on natural products and bioactive compounds of plant origin [12].

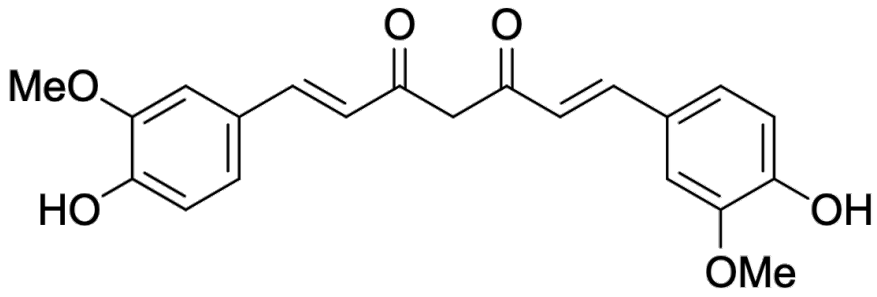


**Figure 1.** Two-dimensional illustration of curcumin.

In summary, its chemical structure is characterized by axial molecular symmetry, composed of terminal phenolic groups and a conjugated β-diketone chain, a feature that confers high chemical reactivity to the molecule and favors interactions with various biological targets, including proteins, enzymes, and nucleic acids [11,13].

These interactions are directly associated with the mechanisms of action of curcumin, resulting in the modulation of fundamental cellular processes, the inhibition of inflammatory pathways, and the regulation of systems involved in redox balance and cellular antioxidant response [14,15].

However, the therapeutic application of curcumin is significantly limited by factors such as its low solubility in aqueous media, reduced systemic bioavailability, and rapid metabolism in vivo [11,16]. Given these limitations, the synthesis and evaluation of structural derivatives of curcumin have been widely used as rational strategies for optimizing its pharmacokinetic properties and biological activity [17,18].

These structural modifications aim to generate compounds with greater chemical and metabolic stability, a better absorption profile, and improved affinity for specific molecular targets, including enzymes involved in cellular detoxification processes, thus expanding their potential for application as bioactive agents [15,19]. In this context, curcumin and its derivatives have been extensively investigated for their ability to act as reactive oxygen species (ROS) scavengers and modulators of endogenous antioxidant systems, since these compounds can stimulate the expression and activity of crucial antioxidant enzymes, such as superoxide dismutase [20], catalase [21], and glutathione *S*-transferase (GST) [22], playing a central role in maintaining cellular homeostasis and highlighting the natural defense mechanisms against oxidative stress.

Despite this, a systematic computational evaluation of structurally substituted curcumin derivatives targeting GST-related antioxidant mechanisms in crustaceans under WSSV-associated oxidative stress has not yet been reported.

Thus, computational approaches have established themselves as strategic tools in the screening of bioactive compounds with antioxidant potential, offering a rational and promising strategy for the development of new alternatives aimed at controlling and mitigating the pathogenic agents in shrimp farming. Thus, this study aims to investigate, using advanced molecular modeling techniques, the structural effect of different substituent groups (R = H−, Br−, Cl−, F−, $NO_2$−, $CH_3$−, and OH−) (Figure 2) [23] on curcumin derivatives on their antioxidant potential and ability to modulate endogenous antioxidant systems, aiming to identify compounds with greater chemical stability, affinity for molecular targets involved in cellular detoxification processes, and applicability in strategies to mitigate oxidative stress in farmed crustaceans.

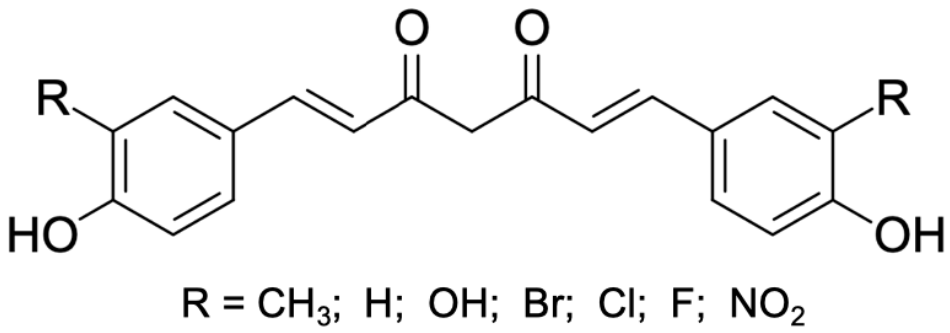


**Figure 2.** Chemical structures of the curcumin derivatives studied. The substituent group (R) varies among H, Br, Cl, F, $NO_2$, $CH_3$, and OH.

## 2. Results

### *2.1. Bioactivity in CUR Derivatives*

In general, predictive data on biological activity indicate that curcumin derivatives have distinct antioxidant profiles, strongly dependent on the chemical modifications introduced into the curcumin skeleton. Considering the set of activities related to oxidative stress, including reducing capacity, free radical scavenging, general antioxidant activity, oxygen scavenging, and modulation of enzymes associated with detoxification, there is a clear differentiation between hydroxylated, alkylated, halogenated, and nitrosated derivatives.

The reducing capacity (Reductant) showed high values for most derivatives, especially CURCH (0.95), CUROH (0.92), and CURNO (0.92), which were higher than the original curcumin (0.86). This behavior suggests that modifications that increase electronic density or favor electron donation contribute positively to this property, which is essential in antioxidant mechanisms based on electron transfer. In contrast, the halogenated derivatives (CURBr, CURCl, and CURF) exhibited significantly lower values (≈0.62), indicating an unfavorable effect of halogenation on the reducing potential, (Table 1).

Regarding free radical scavenger activity, curcumin maintained relatively high values (0.76), while the CURH, CURCH, and CUROH derivatives showed a slight reduction, but still within a biologically relevant range (0.67–0.71). Again, the halogenated derivatives exhibited inferior performance (0.44–0.50), suggesting lower efficiency in the direct neutralization of radical species. CURNO (0.62) showed intermediate performance, indicating that the introduction of the nitroso group maintains moderate antioxidant capacity, possibly associated with alternative redox mechanisms, Table 1.

**Table 1.** Prediction targets and biological (*pa:* to be active and *pi:* to be inactive) activity of CUR derivatives.

| Activity | CUR | CURH | CURCH | CUROH | CURBr | CURCl | CURF | CURNO |
|---|---|---|---|---|---|---|---|---|
| Reductant | 0.86 ± 0.003 | 0.91 ± 0.003 | 0.95 ± 0.002 | 0.92 ± 0.003 | 0.62 ± 0.010 | 0.62 ± 0.010 | 0.62 ± 0.010 | 0.92 ± 0.003 |
| Antimutagenic | 0.81 ± 0.004 | 0.79 ± 0.004 | 0.76 ± 0.002 | 0.81 ± 0.004 | 0.42 ± 0.020 | 0.52 ± 0.014 | 0.46 ± 0.017 | 0.37 ± 0.027 |
| GST substrate | 0.18 ± 0.087 | 0.80 ± 0.003 | 0.80 ± 0.002 | 0.83 ± 0.001 | 0.93 ± 0.002 | 0.85 ± 0.003 | 0.74 ± 0.004 | 0.78 ± 0.004 |
| GST M substrate | 0.77 ± 0.003 | 0.80 ± 0.002 | 0.60 ± 0.005 | 0.82 ± 0.002 | 0.57 ± 0.007 | 0.65 ± 0.004 | 0.75 ± 0.003 | 0.80 ± 0.002 |
| GST A substrate | 0.78 ± 0.004 | 0.88 ± 0.004 | 0.80 ± 0.009 | 0.82 ± 0.005 | 0.87 ± 0.004 | 0.87 ± 0.004 | 0.77 ± 0.012 | 0.90 ± 0.003 |
| GST P substrate | 0.18 ± 0.096 | 0.84 ± 0.004 | 0.81 ± 0.002 | 0.84 ± 0.001 | 0.81 ± 0.002 | 0.81 ± 0.002 | 0.82 ± 0.002 | 0.83 ± 0.001 |
| Free radical scavenger | 0.76 ± 0.003 | 0.67 ± 0.004 | 0.68 ± 0.004 | 0.71 ± 0.004 | 0.46 ± 0.013 | 0.50 ± 0.010 | 0.44 ± 0.014 | 0.62 ± 0.005 |
| Chemopreventive | 0.69 ± 0.007 | 0.65 ± 0.004 | 0.61 ± 0.004 | 0.66 ± 0.004 | 0.32 ± 0.034 | 0.37 ± 0.026 | 0.36 ± 0.027 | 0.37 ± 0.025 |
| Oxygen scavenger | 0.65 ± 0.013 | 0.68 ± 0.008 | 0.68 ± 0.008 | 0.66 ± 0.011 | 0.54 ± 0.039 | 0.53 ± 0.039 | 0.441 ± 0.014 | 0.46 ± 0.064 |
| Antioxidant | 0.61 ± 0.004 | 0.63 ± 0.004 | 0.61 ± 0.004 | 0.74 ± 0.004 | 0.44 ± 0.009 | 0.47 ± 0.008 | 0.45 ± 0.009 | 0.49 ± 0.007 |
| NOS * | 0.27 ± 0.011 | 0.30 ± 0.006 | 0.26 ± 0.015 | 0.29 ± 0.009 | 0.21 ± 0.040 | 0.21 ± 0.040 | 0.21 ± 0.040 | 0.24 ± 0.021 |
| Peroxidase inhibitor | 0.55 ± 0.032 | 0.60 ± 0.025 | 0.26 ± 0.073 | 0.74 ± 0.003 | 0.46 ± 0.013 | 0.61 ± 0.005 | 0.16 ± 0.113 | 0.41 ± 0.015 |

* Notes: NOS—Nitric oxide scavenger.

The overall antioxidant activity (Antioxidant) shows a significant gain for CUROH (0.74), which surpasses all other compounds, including curcumin. This result points to a relevant role of the additional hydroxyl group in the stabilization of reactive species. On the other hand, halogenated derivatives again showed reduced values (≈0.44–0.47), reinforcing a consistent trend of decreased overall antioxidant activity in this group. CURNO (0.49) maintained activity lower than curcumin but higher than some halogenated derivatives, suggesting a balance between positive and limiting structural effects, Table 1.

Oxygen scavenger analysis reveals relatively homogeneous values between CUR, CURH, CURCH, and CUROH (0.65–0.68), while halogenated derivatives and CURNO exhibited reduced activity, especially CURF (0.44) and CURNO (0.46). This pattern suggests that modifications that reduce polarity or introduce electronegative atoms may compromise interaction with reactive oxygen species, Table 1.

Activities related to glutathione S-transferase (GST) deserve mention in the context of indirect antioxidants. The original curcumin showed low probability as a general substrate and for GST P, while most derivatives exhibited high values (>0.80), indicating greater potential for participation in GSH-dependent detoxification pathways. This effect is particularly evident for CURH, CUROH, CURNO, and the halogenated derivatives (CURBr and CURCl), which also display comparable or higher predicted activities in some GST-related endpoints (Table 1). These results suggest that structural modifications, including additional hydroxyl or halogen substituents, favor recognition by GST isoforms and may indirectly enhance cellular protection against oxidative damage.

Finally, peroxidase inhibition showed variable behavior. CUROH (0.74) stood out again with greater inhibitory potential, while CURCH and CURF showed low values, indicating that not all structural modifications favor this specific antioxidant mechanism. CURNO (0.41) showed moderate activity, consistent with its intermediate antioxidant profile observed in other categories, Table 1.

The comparison between CURH and CUROH derivatives provides insight into the influence of additional hydroxyl (OH) groups on the predicted antioxidant activity of curcumin derivatives. PASS predictions indicate that CUROH, which contains an extra OH group compared to CURH, has slightly higher Pa values for antioxidant activity, suggesting a modest enhancement in predicted activity. QSAR descriptors further support this observation, reflecting minor changes in electronic and hydrophilic properties associated with the additional hydroxyl group. Together, these findings underscore how specific structural modifications can affect the predicted antioxidant potential of curcumin derivatives.

Consistent with this, the results indicated that hydroxylated and alkylated derivatives tend to enhance antioxidant activity, both directly and indirectly, compared to the original curcumin, while halogenated derivatives exhibit an overall negative impact on multiple

antioxidant mechanisms. CURNO, in turn, has a moderate and diversified antioxidant profile, combining good reducing capacity and involvement in GST-mediated detoxification pathways, albeit with limitations in direct scavenging activities.

### *2.2. Correlation Between EA vs. pKi*

Docking simulations of the *Lv*GSTMu protein with the co-crystallized ligand GSH and different curcumin (CUR) derivatives revealed significant differences in affinity energy, inhibition constant, pKi, and RMSD. The *Lv*GSTMu–GSH complex had an affinity energy of −5.4 kcal/mol, Ki of $1.09 \times 10^{-4}$ M, pKi of 3.96, and RMSD of 1.960 Å, serving as a reference for docking validation. All CUR derivatives exhibited more negative affinity energies than GSH, ranging from −7.2 to −8.5 kcal/mol, indicating more energetically favorable interactions with the active site of *Lv*GSTMu, Table 2.

**Table 2.** Affinity, Ki, pKi and RMSD energy values of the complexes formed after docking simulations against the *Lv*GSTMu enzyme.

| Complex | Energy (kcal/moL) | $K_i$ (*M*) | $pK_i$ | RMSD (Å) |
|---|---|---|---|---|
| GSH/*Lv*GSTMu | −5.4 | $1.09 \times 10^{-4}$ | 3.96 | 1.960 |
| CUR */*Lv*GSTMu | −7.2 | $5.24 \times 10^{-6}$ | 5.28 | 0.789 |
| CURH/*Lv*GSTMu | −7.3 | $4.43 \times 10^{-6}$ | 5.35 | 1.391 |
| CURCH/*Lv*GSTMu | −7.8 | $1.90 \times 10^{-6}$ | 5.72 | 1.745 |
| CUROH/*Lv*GSTMu | −7.7 | $2.25 \times 10^{-6}$ | 5.65 | 1.155 |
| CURBr/*Lv*GSTMu | −7.6 | $2.67 \times 10^{-6}$ | 5.57 | 1.662 |
| CURCl/*Lv*GSTMu | −7.7 | $2.25 \times 10^{-6}$ | 5.65 | 1.733 |
| CURF/*Lv*GSTMu | −7.6 | $2.67 \times 10^{-6}$ | 5.57 | 1.924 |
| **CURNO/*Lv*GSTMu** | −8.5 | $5.83 \times 10^{-7}$ | **6.23** | 1.081 |

* Comparative control. Notes: Ki, inhibition constant; pKi, inhibition potential (logarithm of the inhibition constant, Ki); and RMSD, root mean square deviation.

Among them, the CURNO derivative had the highest estimated affinity, with an EA of −8.5 kcal/mol, Ki of $5.83 \times 10^{-7}$ M, and pKi of 6.23, accompanied by an RMSD of 1.081 Å, suggesting good structural stability and reliability of the pose obtained. Other derivatives, such as CURCH and CUROH, also stood out, with EA between −7.7 and −7.8 kcal/mol and RMSD below 1.8 Å, indicating reliable and energetically favorable poses. RMSD was used as a criterion for selecting the most reliable conformations, considering values below 2.0 Å as indicative of reproducible poses consistent with the orientation of the ligand in the active site, Table 2.

The integrated analysis of affinity energy ($E_A$), Ki (inhibition constant), pKi (inhibition potential), and RMSD (Root Mean Square Deviation) allows for a detailed understanding of both the affinity and structural reliability of protein–ligand complexes. All curcumin derivatives had pKi values greater than 5.0, confirming micromolar to nanomolar affinity, significantly higher than that of GSH, whose pKi is 3.96. These data indicate that CUR derivatives can bind with greater affinity to the active site of *Lv*GSTMu, with CURNO being the most promising candidate. The relatively low RMSD value observed for CUR * (0.789 Å) shows excellent overlap of the pose with the ideal position, reinforcing the robustness of the prediction, while derivatives such as CURF and GSH itself have higher RMSD values, still within the acceptable limit, but suggesting lower structural consistency, Table 2.

Furthermore, the correlation between EA, pKi, and RMSD allows us to identify not only energetically favorable ligands but also structurally reliable ones. Derivatives such as CURNO, CUROH, and CURCH have more negative EA and RMSD within acceptable limits, indicating a high probability of efficient occupation of the active site and stabilization of the complex. In contrast, GSH, although physiologically relevant, has lower computational

affinity and relatively high RMSD, suggesting that CUR derivatives may surpass the affinity of the co-crystallized ligand. Together, the results indicate that curcumin and its derivatives, especially CURNO, CUROH, and CURCH, have the potential to modulate or inhibit *Lv*GSTMu, standing out as promising candidates for future studies of molecular interaction and inhibitor development.

### *2.3. Comparative Analysis Between GSH (Co-Crystallized) and CUR (Comparative Control)*

Molecular docking simulations performed with the *Lv*GSTMu protein allowed detailed characterization of the intermolecular interactions established by the ligands GSH (co-crystallized) and curcumin (CUR) at the binding site, Figure 3a. Initially, the CUR compound (majority comparative) adopted a spatial orientation analogous to that of the reference crystallographic ligand (GSH) within the catalytic cavity. A significant overlap was observed between the binding poses of CUR and GSH, suggesting that the comparative compound can exploit the same interaction microenvironment and preserve the structural contacts essential for molecular recognition at the active site, Figure 3b.

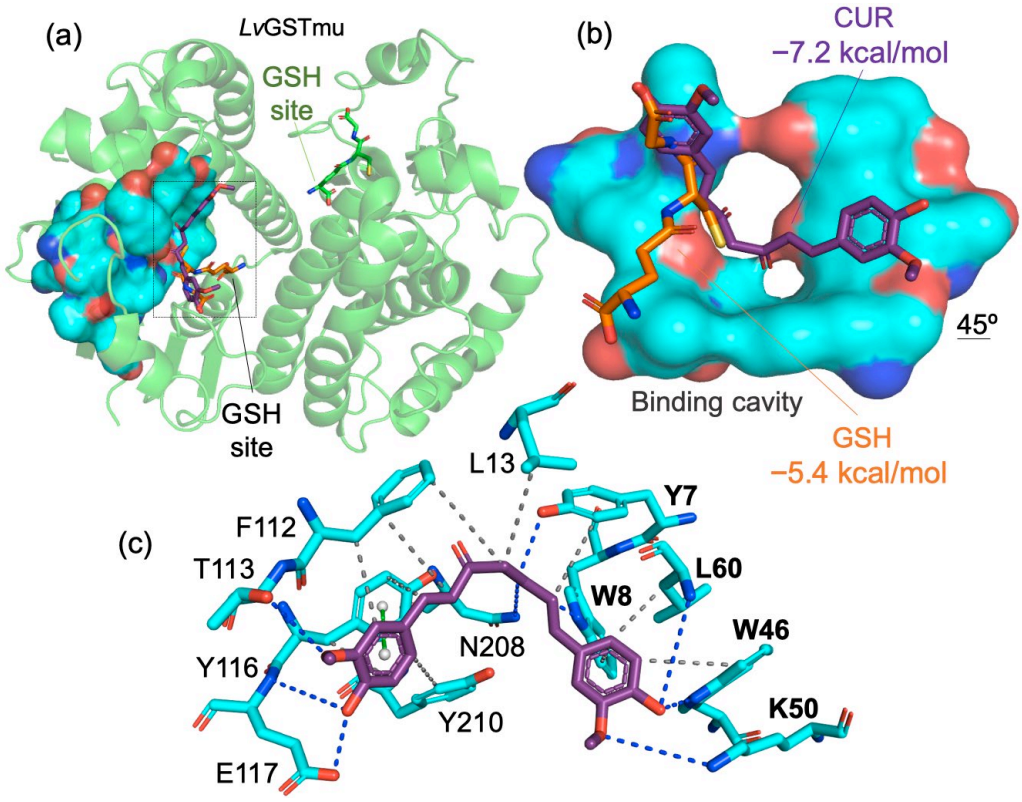


**Figure 3.** (**a**) Global localization of ligands, (**b**) Extended vision between GSH (orange, Table 3) and CUR (purple), and (**c**) Interactions between GSH and e CUR (hydrophobic—gray, H-bond—dark blue, and π-Stacking—green).

The *Lv*GSTMu–GSH complex presented a pattern of interactions dominated by hydrogen bonds and salt bridges, involving polar and charged residues of the active site, such as Y7, W8, Q72, S73, K50, and K74, with distances ranging from 1.15 to 4.23 Å. Noteworthy is the strong hydrogen bond between GSH and W8, with a minimum distance of 1.15 Å, in addition to the formation of salt bridges with K50 and K74, suggesting high electrostatic complementarity, Table 3.

**Table 3.** Data on ligand–receptor (L-R) interaction in the redocking process of the GSH and molecular docking of the CUR (curcumin, comparative).

| Compd | Inter. Type | Residues Distances (Å) |
|---|---|---|
| GSH | H-bond | **Y7** (3.82), **W8** (1.15), K43 (4.00), **W46** (2.19), **L60** (4.23), Q72 (3.38), Q72 (2.15), S73 (1.73), K74 (3.61) |
| | Salt bridge | **K50** (3.83), K74 (3.61) |
| CUR | Hydrophobic | Y7 (4.27), Y7 (4.50), W8 (4.22), L13 (4.67), W46A (4.79), L60 (3.55), F112 (4.95), F112 (4.81), F112 (3.74), Y116 (3.63), Y116 (3.93), Y210 (4.84) |
| | H-bond | **Y7** (2.13), **W8** (3.25), **W46** (2.20), **K50** (3.77), **L60** (4.29), T113A (3.29), E117 (3.83), E117 (2.64), N208 (3.55) |
| | π-Stacking | Y116A (4.20) |

In turn, the *Lv*GSTMu–CUR complex exhibited a more diverse interaction profile, combining hydrophobic interactions, hydrogen bonds, and π-stacking interactions. Curcumin interacted with aromatic and hydrophobic residues, including Y7, W8, W46, L60, F112, Y116, and Y210, with distances between 2.13 and 4.95 Å. The most relevant hydrogen bonds were observed with Y7 (2.13 Å) and W46 (2.20 Å), while π-stacking interactions with Y116 contributed to the stabilization of the complex, Figure 3c.

Comparative analysis revealed that both ligands share a set of common residues at the binding site, notably Y7, W8, W46, L60, and K50, indicating that curcumin occupies a similar spatial region to that of the co-crystallized ligand GSH at the active site of *Lv*GSTMu, Figure 3c.

### *2.4. NMA-Based Dynamic*

Molecular dynamics (MD) simulations coupled with a Normal Mode Analysis (NMA) module were conducted to investigate the structural deformability of the ligand–protein complex formed between the GSH and CUR compounds and the *Lv*GSTmu enzyme target.

The results indicated that the application of the NMA module to the crystallographic structure of *Lv*GSTmu (PDB ID: 5AN1) revealed mean root mean square (RMS) displacement values ranging from ~0.5 to 1.0 Å. A significant contribution of conformational fluctuations was observed in the Cα atoms, with amplitudes around 0.6 Å concentrated in the region corresponding to the sequence of residues 1–2, Figure 4a.

Additionally, more pronounced conformational variations were identified in the regions between residues 40, 57, 67, 121, 176, and 201, as highlighted by the black line, presenting deformation amplitudes between 0.6 and 1.0 Å (Figure 4a). These regions coincide with the functionally relevant binding site of *Lv*GSTmu, previously described as the substrate recognition cavity, whose interaction interface was estimated at 159.74 $Å^2$ (Figure 4a). These results suggest that these structural regions play a central role in the conformational flexibility of the catalytic domain and in the accommodation of the ligands studied.

The application of Normal Mode Analysis (NMA) in the presence of the reference inhibitor GSH (green line) resulted in a subtle structural modulation in the interface area of the complex, indicating a conformational deviation in the conformation of the catalytic domain. Consistent with this, the conformational behavior of *Lv*GSTmu in the presence of the co-crystallized ligand GSH shows average RMS values below 1.0 Å for the terminal region between residues 40 and 57, Figure 4a.

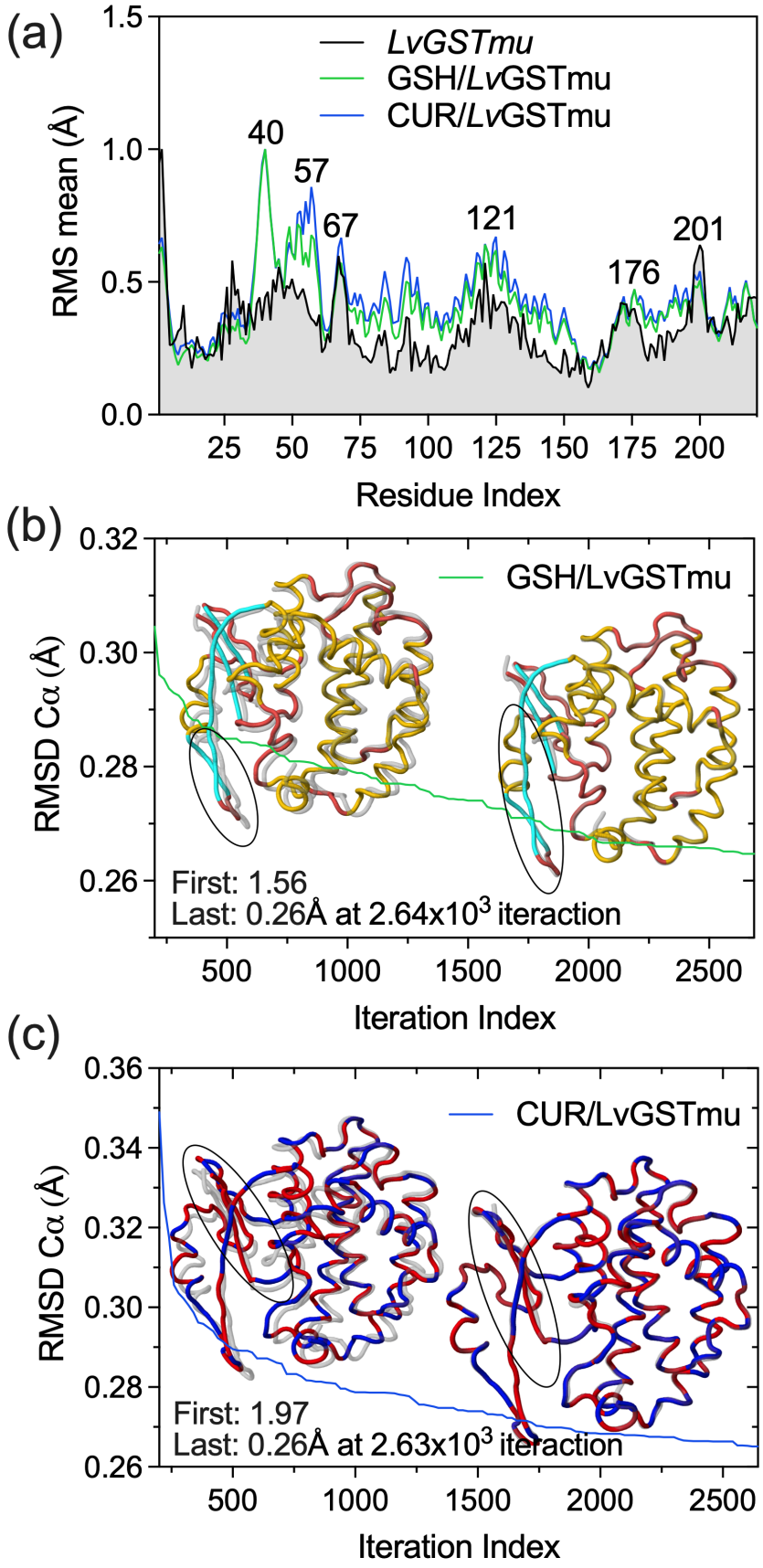


**Figure 4.** (**a**) Normal mode analysis (NMA) showing intrinsically flexible regions of the *Lv*GSTmu subunit (black line); (**b**) The GSH/*Lv*GSTmu complex converged to a final RMSD of 0.26 Å in ~2.6 × $10^3$ iterations; and (**c**) The CUR/*Lv*GSTmu complex converged to a final RMSD of 0.26 Å in ~2.6 × $10^3$ iterations.

For the trajectory of the GST/*Lv*GSTmu complex (green line), an initial RMSD of approximately 1.56 Å was analyzed, followed by a convergence process over ~2.64 × $10^3$ iterations (calculation steps), culminating in a final RMSD of around 0.26 Å (Figure 4b). Thus, RMSD values ranged from 2.0 to 3.0 Å, indicating physiologically marked conformational fluctuations indicating excessive distortion events.

Notably, the CUR (curcumin) comparison induced more pronounced conformational shifts in the Cα atoms of region 57–67, presenting average RMS values around ~0.65 Å (Figure 4a), which suggests greater local disturbance of the structural architecture of the catalytic site. In contrast, in the presence of the CUR compound (blue line), an average RMS value of approximately 0.5 Å was observed, indicating a more significant conformational profile and suggesting that GSH and CUR compete for the same binding site. Nevertheless, the data show that CUR promotes a more pronounced global structural disruption of the system when compared to GSH, reflecting relevant differences in the ligand–protein interaction mechanisms, Figure 4a.

Similarly, the CUR/LvGSTmu complex (blue line) had an initial RMSD of approximately 1.97 Å, stabilizing at a final RMSD of 0.26 Å after approximately 2.63 × $10^3$ iterations (Figure 4c). This behavior suggests that the CUR/*Lv*GSTmu complex required a greater number of iterative cycles to reach convergence when compared to the CUR/*Lv*GSTmu complex. Together, the results of NMA-based MD simulations indicate that the collective movements associated with both complexes are structurally stable and remain within a dynamic regime compatible with the physiological functionality of the receptor.

### *2.5. Ecotoxicological Analysis*

The physicochemical properties of curcumin and its derivatives were evaluated in order to understand how structural modifications influence parameters directly associated with the environmental and ecotoxicological behavior of these compounds. Based on the results obtained using JANUS software Version 1.0.3, Table S1 was prepared, presenting the logKow values, water solubility, and parameters related to persistence and toxicity, enabling a comparative analysis between curcumin and its structural analogs.

Curcumin (CUR) had a logKow value of 1.81, classifying it as a compound with moderate lipophilicity (1 < logKow < 2), a characteristic that indicates affinity for both the aqueous phase and organic compartments, such as sediments and soils [24,25]. This behavior is corroborated by the observed solubility (61.9 mg/L), which suggests a reasonable ability to remain in the aqueous phase, favoring its dispersion in the aquatic environment [26].

Among the derivatives analyzed, CURH and CUROH presented logKow values close to that of curcumin (2.01) but with a significant increase in solubility, especially in the case of CUROH, which presented a value greater than 900 mg/L. This result indicates that the introduction of more polar groups favors interaction with water, reducing the tendency to partition into hydrophobic compartments. The high solubility of these derivatives suggests a lower propensity for bioaccumulation, since highly soluble compounds tend to remain predominantly dissolved in the aquatic environment [27].

In contrast, halogenated derivatives (CURBr, CURCl, and CURF) showed a significant increase in logKow, with values ranging from 3.30 to 3.52, characterizing more lipophilic compounds. These values indicate greater affinity for sediments and soils, as well as greater potential for interaction with biological membranes, a behavior widely described for halogenated organic compounds [28]. In addition, these derivatives showed low water solubility values, below 10 mg/L, evidencing the tendency to partition into solid and biological phases.

The CURCH derivative showed intermediate behavior, with a logKow value of 2.77 and reduced solubility (16.53 mg/L), indicating that small structural changes are suffi-

cient to promote significant changes in the hydrophilic-lipophilic balance of the molecule. Similarly, the CURNO derivative showed intermediate logKow (2.37) and moderate solubility, reflecting a physicochemical profile distinct from both curcumin and more lipophilic derivatives.

The bioaccumulation potential of curcumin and its derivatives was assessed using the bioconcentration factor (BCF) and bioaccumulation factor (BAF), as shown in Table S1. In general, the values obtained indicated low bioaccumulative potential for most of the compounds evaluated, with the exception of some derivatives that presented intermediate values, still below the limits considered worrisome from a regulatory point of view [29,30].

The assessment of the environmental persistence of curcumin derivatives showed significant variations between the compartments analyzed, with generally low stability in water and soil and greater retention in sediment for specific compounds. All derivatives had aquatic half-lives of less than 40 days, classifying them as non-persistent (nP) in water, which suggests rapid degradation in this medium and reduced potential for chronic exposure to organisms in the water column. In soil, most substances were also classified as non-persistent, with half-life values well below the 120-day threshold. Only the CURCl derivative had a value close to this limit (117 days), indicating greater relative stability, although still below the regulatory criterion for persistence [31].

Sediment stood out as the compartment with the highest environmental retention. The CURH and CURNO compounds had half-lives of 227 days, exceeding the threshold of 180 days established for very persistent substances (vP). This result indicates that these derivatives can remain for long periods in benthic environments, acting as environmental reservoirs. In contrast, the other compounds exhibited half-lives in sediment of less than 120 days, remaining in the non-persistent category. Thus, the environmental persistence of the evaluated derivatives is compartment-dependent, with greater ecotoxicological relevance for sediments than for water or soil [32].

The bioconcentration (BCF) and bioaccumulation (BAF) factors estimated for all compounds remained well below the threshold of 5000 L/kg for classification as bioaccumulative. The values observed ranged from 0.9 to 61 L/kg, characterizing low to negligible bioaccumulation potential. The highest values were observed for CURH, CURF, and CURCH, but still within a range considered ecotoxicologically low. On the other hand, halogenated derivatives such as CURBr, CURCl, and CURNO had values below 1 L/kg, indicating virtually no biological retention [33].

The comparison between BCF and BAF revealed very similar values for all compounds, indicating that trophic incorporation does not contribute significantly to body accumulation. This equivalence suggests an absence of biomagnification along the food chain and that the accumulation observed results mainly from direct absorption from the environment, followed by efficient elimination, i.e., this behavior indicates that organisms have the ability to metabolize or excrete these derivatives relatively quickly [34].

Joint analysis of persistence and bioaccumulation data shows a clear dissociation between environmental retention and biological retention. Although CURH and CURNO are classified as very persistent in sediment, their BCF and BAF values remain low, demonstrating that prolonged permanence in the environment does not translate into significant accumulation in organisms [29,35]. This pattern indicates that the observed persistence is associated with stability in the abiotic compartment, without implying an increased risk of biomagnification or prolonged trophic exposure. For the other compounds, the combination of low persistence and low bioaccumulation factors provides a favorable environmental profile.

## 3. Discussion

### *3.1. Inhibition Potential vs. Selectivity*

Statistical analysis of the average affinity energies ($E_A$) obtained for curcumin and its derivatives revealed highly significant differences in relation to the co-crystallized ligand GSH. Applying a one-way ANOVA test, followed by Dunnett's multiple comparisons test, all comparisons between GSH and the derivatives showed adjusted values of $p < 0.0001$, indicating that the difference in average affinity between the groups did not occur by chance, Figure 5a.

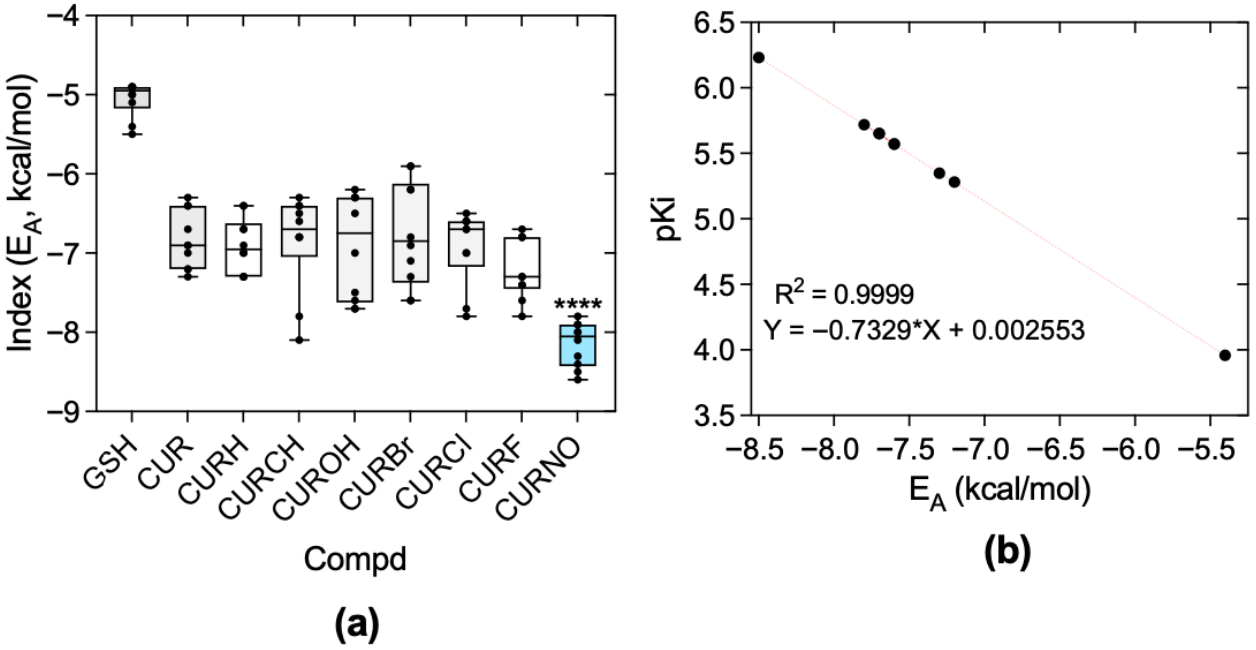


**Figure 5.** (**a**) Analysis of variance (ANOVA) of binding energies ($p < 0.05$). The values group represents the mean ± standard error (GSH and CUR derivatives), **** $p < 0.0001$. (**b**) Correlation between pKi and affinity energy analyzed by linear regression.

The mean differences (Mean Diff.) ranged from 1.70 kcal/mol for CURBr to 3.10 kcal/mol for CURNO, with 95% confidence intervals clearly above the significance threshold, confirming the robustness of the observed differences. These statistical results corroborate that curcumin derivatives have significantly higher affinity for the active site of *Lv*GSTMu compared to the co-crystallized ligand, suggesting that functional modifications applied to the CUR molecule may contribute to increased molecular complementarity and stability of the protein-ligand complex, Figure 5a.

In summary, ANOVA analysis followed by multiple comparisons revealed a consistent pattern: all CUR derivatives significantly outperform GSH in terms of average binding energy, with CURNO showing the greatest effects in relation to the reference ligand.

Linear regression analysis between the affinity energy ($E_A$) obtained in docking simulations and the pKi of curcumin derivatives revealed an extremely robust correlation between the two variables. The model showed a nearly perfect fit, indicating that the variation in pKi is almost entirely explained by the variation in $E_A$, Figure 5b. The slope of the line was significantly different from zero, evidencing a direct and consistent linear relationship between binding energy and estimated affinity. The equation obtained demonstrated an inverse relationship between EA and pKi, as expected thermodynamically, showing that more negative affinity energy values correspond to higher pKi, reflecting greater affinity for the active site of *Lv*GSTMu, Figure 5b. These results show that the affinity energies obtained

in docking can be used as reliable quantitative predictors of ligand affinity, describing the prioritization of the most promising curcumin derivatives, such as CURNO, for subsequent stages of molecular docking and dynamics.

### *3.2. Behavior of Biochemical Interactions via LvGSTmu*

A comprehensive description of the molecular interactions between the curcumin derivatives and the target protein is presented in Appendix A.

Analysis of intermolecular interactions suggests that GSH, as a co-crystallized physiological ligand, establishes a highly specific binding pattern with *Lv*GSTMu, characterized by short hydrogen bonds and salt bridges, reflecting strong electrostatic stabilization of the complex. The presence of distances shorter than 2.0 Å, particularly with residue W8, indicates highly favorable interactions consistent with the typical catalytic function of glutathione *S*-transferases.

In contrast, curcumin exhibits a distinct binding mode, although partially overlapping with that of GSH. The recurrent involvement of aromatic residues, such as Y7, W8, W46, F112, and Y116, shows that the stabilization of the *Lv*GSTMu–CUR complex is predominantly mediated by hydrophobic and π-π interactions, with a complementary contribution from hydrogen bonds. This profile is consistent with the hydrophobic and polycyclic nature of curcumin, which favors interactions with nonpolar regions of the active site.

The identification of common residues among the complexes, especially Y7, W8, and W46, suggests that curcumin may partially compete with GSH for the binding site or modulate the activity of *Lv*GSTMu by occupying the same structural microenvironment. However, the absence of salt bridges and the lower predominance of electrostatic interactions compared to GSH indicate differences in the degree of affinity and in the stabilization mechanism of the complex, Table 4.

**Table 4.** Data on ligand–receptor (L-R) interaction in the redocking process of the GSH (co-crystallized) and molecular docking of the CURNO (drug candidate).

| Compd | Inter. Type | Residues Distances (Å) |
|---|---|---|
| GSH | H-bond | **Y7** (3.82), **W8** (1.15), K43 (4.00), **W46** (2.19), **L60** (4.23), Q72 (3.38), Q72 (2.15), S73 (1.73), K74 (3.61) |
| | Salt bridge | **K50** (3.83), K74 (3.61) |
| CURNO | Hydrophobic | Tyr7 (4.73), Leu13 (3.77), Leu13 (4.08), Phe112 (3.48), Phe112 (3.49), Tyr116 (4.38), Tyr116 (3.61), Tyr116 (3.70), Tyr116 (4.30) |
| | H-bond | Tyr7 (1.77), Trp8 (3.21), Leu13 (4.06), Asn59 (2.48), Gln72 (2.84), Asp106 (3.10), Thr113 (2.02) |

Together, these results indicate that, although curcumin does not completely mimic the binding pattern of the co-crystallized ligand, it exhibits energetically favorable interactions and a binding mode compatible with the active site of *Lv*GSTMu, suggesting potential modulatory or inhibitory activity of this enzyme.

The analysis of the protein–ligand complexes revealed that CURNO predominantly occupies the same binding cavity previously identified for crystallized GSH and curcumin (CUR), indicating that this region of the binding site exhibits high structural permissiveness toward ligands with redox-active and aromatic features, Figure 6a. This spatial overlap suggests that CURNO exploits molecular determinants similar to those involved in the recognition of the reference ligands while establishing a distinct interaction pattern driven by the presence of the nitroso moiety, Figure 6b.

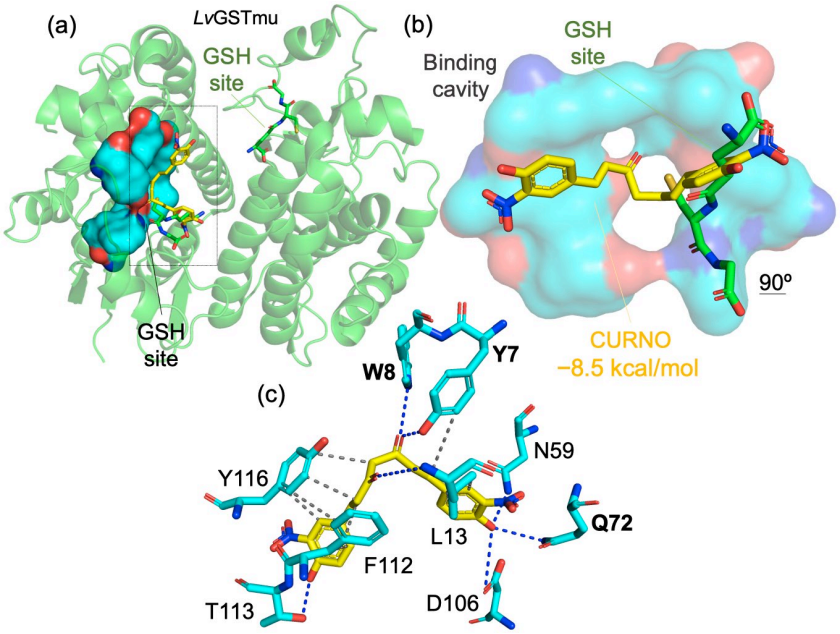


**Figure 6.** (**a**) Global localization of ligands, (**b**) Extended vision between GSH (Table 4, green) and CUR (purple), and (**c**) Interactions between GSH and e CURNO (hydrophobic—gray and H-bond—dark blue).

Overall, in the GSH-bound complex, stabilization is dominated by an extensive hydrogen-bonding network involving Y7, W8, Q72, S73, and K74, complemented by salt bridges with K50 and K74, consistent with the hydrophilic and electrostatic nature of GSH binding. In contrast, CUR displays a more balanced interaction profile, combining hydrophobic contacts with aromatic residues (Y7, W8, F112, and Y116) and hydrogen bonds with Y7, W8, W46, K50, L60, T113, E117, and N208, while a $\pi$-stacking interaction with Y116 further stabilizes its conformation within the binding cavity, Table 4.

The CURNO–protein complex displays a distinct interaction profile, characterized by a predominance of hydrophobic interactions, mainly involving Y7, L13, F112, and Y116, Table 4. The multiple contacts observed with Y116, at varying interaction distances, indicate a central role for this residue in anchoring the aromatic scaffold of CURNO and promoting its alignment along the binding cavity, Figure 6c. The contribution of F112 further evidences the hydrophobic environment, favoring efficient aromatic packing and overall complex stability.

Despite the dominance of hydrophobic interactions, CURNO also establishes directional hydrogen bonds with Y7, W8, N59, Q72, D106, and T113, which appear to play a key role in the fine orientation of the ligand and in stabilizing the nitroso group within the cavity. The recurrent involvement of conserved residues such as Y7 and W8, which are also engaged in the binding of GSH and CUR, underscores the functional importance of these positions in molecular recognition, irrespective of ligand identity, Figure 6a and Table 4.

From a comparative perspective, while GSH relies predominantly on polar and ionic interactions and CUR displays a mixed interaction profile, CURNO preferentially exploits the aromatic and hydrophobic character of the binding cavity without compromising essential directional interactions, Table 4. This reorganization of the interaction balance may be directly associated with the distinct redox behavior of CURNO, as a more hydrophobic microenvironment is known to modulate the electronic stability of nitroso-containing groups and influence electron-transfer processes, Figure 6c.

In a literary context, recent studies show that curcuminoids act as relevant modulators of the antioxidant system in aquatic organisms. In *L. vannamei*, supplementation with turmeric and curcumin has been associated with increased resilience to saline stress,

accompanied by changes in the activity of glutathione-dependent enzymes, suggesting a functional role for these compounds in regulating redox balance in crustaceans. This pattern indicates that the observed enzymatic modulation is not limited to a nonspecific response to stress but may reflect the activation of endogenous antioxidant mechanisms mediated by compounds with a curcuminoid structure [36].

Findings in *D. rerio* corroborate this interpretation, since curcumin has demonstrated a hepatoprotective effect against oxidative stress associated with the induction of phase II detoxification enzymes and the reduction in biomolecular damage. In this scenario, glutathione *S*-transferase (GST) is often described as a key component of the adaptive response, promoting the conjugation of reactive metabolites and contributing to the maintenance of cellular homeostasis. Thus, variations in GST activity have been interpreted as functional indicators of antioxidant system modulation and not just as markers of toxicity [37].

More broadly, reviews of curcumin's action in different animal groups point to the regulation of evolutionarily conserved redox pathways, including those controlled by transcription factors sensitive to oxidative status. This theoretical framework supports the hypothesis that compounds that preserve the curcuminoid core may influence the antioxidant response through two complementary pathways: direct neutralization of reactive species and induction of enzymes involved in cellular detoxification [38].

### *3.3. Molecular Dynamics (NMA-Mode)*

Given the Normal Mode Analysis (NMA) module applied to the crystallographic structure of the *Lv*GSTmu receptor and the CURNO/*Lv*GSTmu complex, the descriptors were consistent with the other complexes previously analyzed, with only one variation in residue 175, which generally showed values close to RMS around 1.0 Å. Figure 7a.

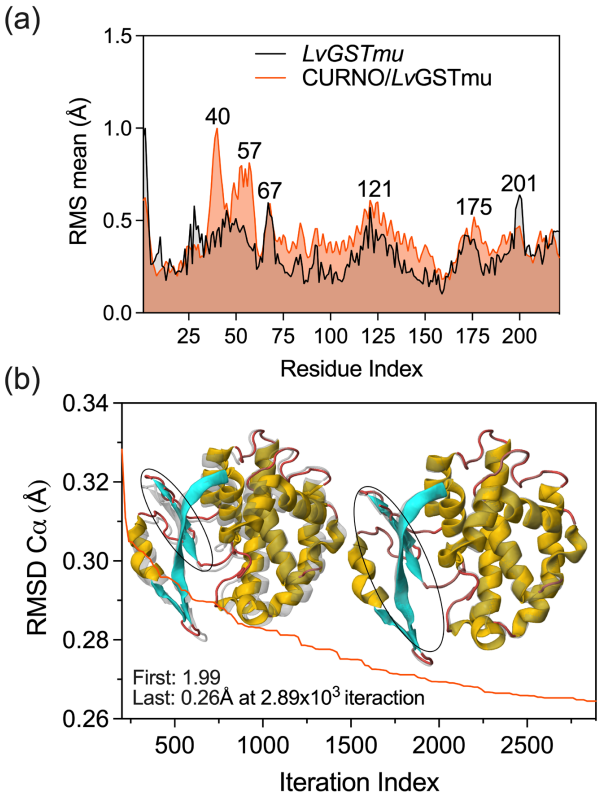


**Figure 7.** (**a**) Normal mode analysis (NMA) showing intrinsically flexible regions of the *Lv*GSTmu subunit (black line); (**b**) The CURNO/*Lv*GSTmu complex converged to a final RMSD of 0.26 Å in ~2.8 × $10^3$ iterations.

In contrast, a slight reduction in structural flexibility was described when the CURNO compound (orange line) was complexed to its respective binding site in chain A (5AN1: A). Under these conditions, the average RMS values were substantially lower than 1.0 Å (Figure 7a), indicating a stabilizing effect induced by the binding of the ligands and a restriction of local movements of the protein skeleton in these regions.

The conformational profile assessment reveals the presence of an energetically viable structural transition pathway between CURNO when complexed to the *Lv*GSTmu receptor (PDB ID: 5AN1). This showed high conformational similarity to the CUR (curcumin) comparative defined in molecular docking simulations, as well as by root mean square deviation (RMSD) values of 0.2644 Å. However, temporal analysis of the RMSD indicates a slightly marked reduction to values close to ~3.0 Å throughout the simulation (Figure 7b), suggesting the occurrence of abrupt and structurally conservative conformational adjustments of the ligand–receptor complex.

This decrease in RMSD is associated with a greater conformational disturbance of the protein's Cα atoms induced by the CURNO ligand, when compared to that observed for the GSH ligand (Figure 5b). The regions subjected to localized conformational twists, highlighted by the indicative circles, reflect structural rearrangements resulting from the formation and stabilization of the ligand–receptor (L–R) complexes. Such rearrangements remain restricted and do not imply global changes in the topology of the binding site.

In the context of the molecular dynamics simulations conducted, RMSD values consistently around 3.0 Å are indicative of structural stability and the absence of abrupt conformational events, corroborating that the fluctuations observed are within a range considered ideal for maintaining the conformational integrity and thermodynamic stability of the CURNO/*Lv*GSTmu complex.

### *3.4. Exposure Acute and ChV Analysis*

The assessment of the acute toxicity of curcumin derivatives revealed consistent interspecific variation, with differences in sensitivity between aquatic trophic levels [39]. Overall, $LC_{50}/EC_{50}$ values were predominantly in the range of 1–10 mg/L, classifying most compounds as toxic to at least one of the organisms tested, Table S1. However, a clear pattern of greater sensitivity was observed among primary organisms and invertebrates when compared to fish [40].

The values for fish (96 h) ranged from 1.10 to 3.33 mg/L, indicating moderate and relatively homogeneous toxicity among the compounds. For DM (48 h), the values were substantially lower (0.0016–0.3554 mg/L), evidencing greater susceptibility of this organism. Green algae (96 h) showed the widest range of response (0.278–14.1 mg/L), reflecting a strong structural dependence on toxicity for primary producers, Table S1.

A direct comparison of $LC_{50}/EC_{50}$ values shows that DM was generally the most sensitive organism to the derivatives evaluated. For all compounds, the values obtained for DM were consistently lower than those observed for fish and, in most cases, also lower than the values for algae. Although some substances also showed high toxicity to algae (values < 1 mg/L), Table S1, the general trend indicates that planktonic invertebrates are the most vulnerable trophic group [41]. Fish, on the other hand, were comparatively less sensitive, with no values below 1 mg/L.

The one-way analysis of variance revealed differences between the groups of organisms, and Tukey's multiple comparison test identified a statistically significant difference between DM and green algae ($p = 0.0320$). This result indicates that, on average, toxicity values for DM are significantly lower than for algae, corroborating the greater sensitivity of invertebrates, Figure 8a.

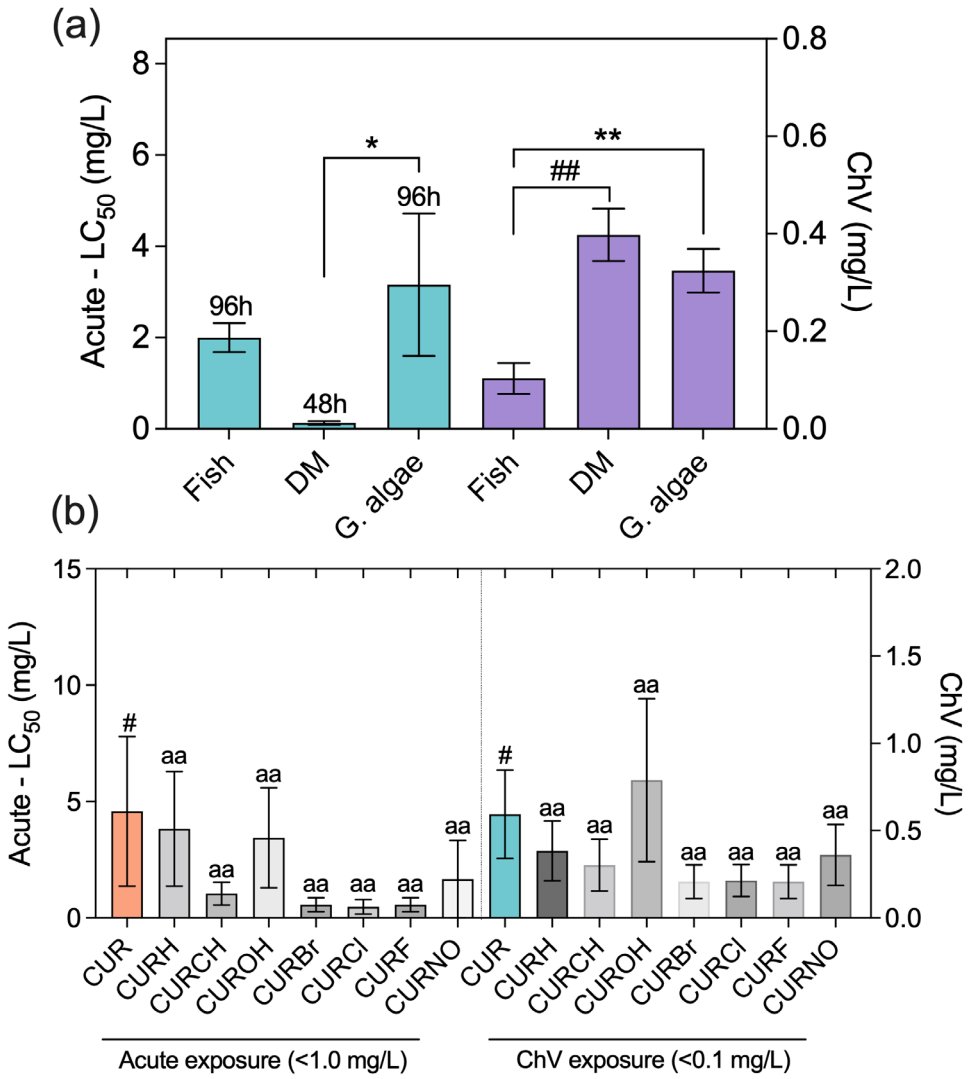


**Figure 8.** (**a**) Comparative analysis of acute and chronic toxicity (fish, *D. magna* and *G. algae*) across groups, * $p < 0.0320$, ## $p < 0.0011$, and ** $p < 0.0023$; # Majority component and (**b**) The values individuals represent the mean ± standard error (not statistically significant—aa) (CUR vs. derivatives).

On the other hand, statistically significant differences were observed between fish and DM ($p = 0.0011$) or between fish and algae ($p = 0.0023$). This suggests that, despite the trend of higher toxicity for DM, intra-group and inter-compound variability reduces the statistical distinction between all trophic levels when compared broadly.

In general, structural modifications can influence toxicity differently between trophic levels. In the case of CURNO, the presence of the nitroso group is associated with lower acute toxicity to fish and algae compared to some analogs, indicating an organism-specific effect of this substitution, Table S1. However, this pattern is not generalizable, as the compound showed extremely high toxicity to DM, evidencing the high sensitivity of aquatic invertebrates [42].

In addition, the literature indicates that nitroso groups may be related to reactive biological activity, including potential mutagenic effects in certain experimental systems [43]. Thus, even when acute toxicity is not the highest for all organisms, the presence of this functional group remains relevant in broader toxicological assessments [44].

The chronic toxicity (ChV) assessment of curcumin derivatives revealed a more pronounced risk profile than that observed for acute toxicity, with effective concentrations mostly below 1 mg/L for all trophic levels. These values classify most compounds as

toxic (0.1–1 mg/L) or very toxic (<0.1 mg/L) under prolonged exposure, indicating that sublethal effects may occur at environmentally relevant concentrations, Table S1. In general, fish showed the lowest ChV values for most derivatives, followed by DM and algae, highlighting differences in susceptibility between groups [45].

For fish, four compounds (CURCH, CURBr, CURCl, and CURF) had ChV values below 0.1 mg/L, indicating very high chronic toxicity. The other derivatives (CUR, CURH, CUROH, and CURNO) ranged from 0.1 to 1 mg/L, still classified as toxic, Figure 8a. This pattern indicates that, although acute toxicity to fish was moderate, the long-term effects are more significant, suggesting a potential impact on growth, development, or reproduction [42].

Accordingly, the mean ChV values for fish were significantly lower than those for DM ($p < 0.01$) and also lower than those for algae ($p < 0.01$). On the other hand, there was no statistically significant difference between DM and algae ($p > 0.05$), Figure 8a. These results corroborate that fish are significantly more sensitive to chronic exposure, while invertebrates and primary producers show responses of similar magnitude [46].

Furthermore, when the compounds were analyzed individually for effective concentrations in both acute and chronic toxicity tests, no statistically significant differences were observed between the derivatives compared to the reference compound (CUR). The multiple comparison test indicated that all mean differences had confidence intervals covering zero and high adjusted *p*-values ($p > 0.05$), demonstrating the absence of statistically relevant variation between CUR and its structural analogs, Figure 8b.

This result suggests that, although there are numerical variations in $LC_{50}/EC_{50}$ and ChV values among the derivatives, these differences are not consistent enough to characterize a compound as significantly more or less toxic than the original curcumin under the conditions and models evaluated. Thus, the structural modifications introduced in the derivatives appear to influence the sensitivity pattern among organisms (as observed in the analyses by trophic group) but do not promote a statistically robust overall change in toxicity when the compounds are compared with each other [47].

## 4. Materials and Methods

### *4.1. Curcumin Derivatives Analyzed*

The curcumin derivatives evaluated in this study were obtained from the study by Yang et al. (2017) [23], which investigated the role of methoxy groups in anti-inflammatory activity and NF-κB signaling. Importantly, these molecules were not synthesized or purchased, and only their chemical structures were used for in silico analyses to explore antioxidant activity in shrimp (*L. vannamei*). Each derivative was assigned a unique identifier to facilitate reference throughout the study.

Curcumin contains two methoxy groups ($-OCH_3$, see Figure 2) on its aromatic rings, yet their contribution to antioxidant effects remains largely unknown. Bisdemethoxycurcumin, in which the methoxy groups are replaced by hydrogens ($-H$, see Figure 2), shows reduced antioxidant and anti-inflammatory activity [48], suggesting that these substituents may be critical for modulating biological activity and warrant computational investigation in crustacean antioxidant systems.

### *4.2. PASS Online Predictions of Biological Activity*

PASS Online (Prediction of Activity Spectra for Substances) (https://way2drug.com/PassOnline/ accessed on 12 March 2026) is a chemoinformatics system developed to predict the spectrum of biological activities of organic compounds based solely on their chemical structure [49]. The PASS methodology is based on the principle that similar chemical

structures tend to exhibit similar biological activities, formalizing this relationship through structural descriptors and probabilistic models [50,51].

The algorithm uses descriptors known as Multilevel Neighborhoods of Atoms (MNA), which encode the chemical environment of each atom in the molecule at different levels of neighborhood [52]. These descriptors allow the molecular structure to be transformed into a mathematical representation comparable to a large database of compounds with previously known biological activities [53].

The prediction of activities is expressed by two complementary probabilities: Pa (Probability to be Active) and Pi (Probability to be Inactive) [54]. These probabilities are calculated based on statistical models derived from *Bayesian* theory, considering the frequency of occurrence of certain structural descriptors in active and inactive compounds for a given biological activity [52,55]. In simplified terms, the probability of a compound exhibiting a specific activity can be represented as:

$$Pr_j = \left(1 + \left(s_j - s_{0j}\right) / \left(1 - s_j s_{0j}\right)\right) / 2 \quad (1)$$

$s_j$ composite score for activity j, based on the MNA descriptors. $s_{0j}$ training reference score (the threshold between active and inactive) and $P_{rj}$ final probability of activity, normalized between 0 and 1, and considered significant when Pa > Pi, Equation (1).

In addition, the predicted activities were analyzed based on Pa and Pi values, with those having Pa > Pi considered biologically relevant, as higher Pa values indicate a greater probability of experimental confirmation

The values of Pa and Pi do not represent experimental confirmation but rather research priorities. In general, activities with Pa > 0.7 indicate a high probability of experimental manifestation, while intermediate values (0.3 < Pa < 0.7) suggest possible new activities that are still under-explored in the literature [52]. Thus, PASS Online is a robust tool for virtual screening, drug repositioning, and rational experiment planning, reducing costs and time in the initial phase of pharmacological and toxicological research [56].

### *4.3. Ecotoxicological Analysis*

The initial ecotoxicity screening was conducted using the QSAR (Quantitative Structure–Activity Relationship) approach, a widely established chemoinformatics methodology for predicting toxic effects and assessing potential risks associated with chemicals, based exclusively on structural descriptors [57].

ECOSAR (Ecological Structure-Activity Relationship) [58] is a computational model developed by the US Environmental Protection Agency (EPA) used to estimate the toxicity of chemicals in aquatic organisms [59]. Based on the molecular structure of the compounds, ECOSAR applies quantitative relationships known as QSAR (Quantitative Structure-Activity Relationships) to predict effects on fish, crustaceans, and algae [60]. Based on these estimated values, the toxicity of the compounds was classified into different levels, allowing the identification of substances with low, moderate, or high toxic potential, Table 5.

**Table 5.** Quantitative acute and chronic toxicity classification by ECOSAR extension JANUS. Adapted from De Sousa et al. (2026) [61]. * ChV: chronic. Unit: $mg/L^{-1}$.

| Classification | Acute Toxicity | ChV * Toxicity |
|---|---|---|
| Not harmful | $LC_{50}/EC_{50} > 100$ | ChV > 100 |
| Harmful | $10 < LC_{50}/EC_{50} < 100$ | 1 < ChV < 10 |
| Toxic | $1 < LC_{50}/EC_{50} < 10$ | 0.1 < ChV < 1 |
| Very toxic | $LC_{50}/EC_{50} < 1$ | ChV < 0.1 |

This approach is based on establishing quantitative relationships between physicochemical properties, with an emphasis on the octanol/water partition coefficient (logKow), recognized as one of the main determinants of the biological and environmental behavior of organic compounds and observable biological responses, enabling the generation of robust and reproducible toxicity estimates, with a significant reduction in the dependence on extensive experimental testing [62].

$$logLC50 = m \times logKow + b \quad (2)$$

$$ChV = \frac{log\ (NOEC) \times LOEC}{2} \quad (3)$$

$$\log {}^{1}/_{HC_{5aqcom}} = -4.52 + 1.05 \cdot logKow \quad (4)$$

The acute toxicity of the compounds was estimated using Equation (2), in which $y$ corresponds to the concentration associated with the toxic effect ($LC_{50}$, in mg/L) and $x$ represents the octanol/water partition coefficient (logKow), allowing the construction of a linear regression between $LC_{50}$ vs. logKow [61]. Chronic toxicity was calculated using Equation (3), where ChV represents the chronic effect concentration, LOEC the lowest concentration with an observable effect, and NOEC the concentration with no observable effect [63]. Additionally, to evaluate, at different trophic levels, the hazardous concentration for 5% of the aquatic community ($HC_{5aqcom}$ in µmol/L), Equation (4) was used, also considering logKow as an explanatory variable [64,65].

BCFBAF Analysis

BCFBAF consists of a predictive module designed to estimate bioconcentration factors (BCF) and bioaccumulation factors (BAF) in fish organisms, using two independent methodologies. The first is based on an empirical regression model based on the octanol-water partition coefficient (logKow). The second uses the Arnot-Gobas [27] mechanistic model, which explicitly incorporates the dynamics of three trophic levels, as well as the biotransformation rate expressed by the metabolic half-life of the compound.

$$BAF = (1 - L_B) + \frac{K_1 \cdot \phi + (K_D \cdot \beta \cdot \tau \cdot \phi \cdot L_D \cdot Kow)}{(K_2 + K_E + K_G + K_M)} \quad (5)$$

$$BCF = (1 - L_B) + \left( \frac{K_1 \cdot \phi}{K_2 + K_E + K_G + K_M} \right) \quad (6)$$

The value of the factors in the Arnot-Gobas method (Equations (5) and (6)), the variables $1 - L_B$, which refer to the components of the organism, $K_1$, $K_D$, $K_2$, $K_E$, $K_G$, and $K_M$ are used, which, respectively, represent the absorption of compounds by the respiratory surface and diet, as well as elimination through respiration, feces, growth dilution, and metabolic transformation; $\phi$, which refers to the soluble portion of the total concentration in water that can permeate respiratory membranes; $\beta$, which indicates the biomagnification factor; $\tau$, which indicates the degree of trophic dilution; and $L_D$, which represents the lipid content of living beings belonging to a lower trophic level [29,30]. The results follow the standards established by Canada's Environmental Protection Act, which determines when chemicals have the potential for bioconcentration/bioaccumulation, when BCF/BAF $\geq$ 5000 L/Kg [32].

Thus, the prediction was assigned to the structural class most representative of the molecule, considering the similarity index with the highest weight in the model evaluation [66]. Additionally, environmental persistence and half-life values are estimated based on the residence time of the compounds in the environment, expressed in days, classifying substances as non-persistent (nP) or persistent (P) when the half-life exceeds 40 days in

water and 120 days in soil and sediment and as very persistent (vP) when half-life values are greater than 60 days in water and 180 days in soil and sediment [35].

In addition, JANUS software, developed by the German Federal Ministry for the Environment, Nature Conservation, Building, and Nuclear Safety (German UBA), was used to obtain toxicological parameters. The JANUS project (https://www.vegahub.eu/ accessed on 12 March 2026) is an improved version of PROMETHEUS software Version 1.0, expanding its functionality and allowing for more comprehensive assessments [67]. The platform integrates 48 in silico models focused on the analysis of persistence, bioaccumulation, and toxicity (PBT), in addition to providing predictions regarding carcinogenicity, mutagenicity, reproductive toxicity (CMR), and endocrine disruption potential. list the authority that provided approval and the corresponding ethical approval code [68].

### *4.4. Statistical Analysis*

The data were processed using GraphPad Prism (version 8.0.1; GraphPad Software, Inc., La Jolla, CA, USA). Acute and chronic toxicities were assessed for normality using the *Shapiro–Wilk* test ($p > 0.05$). Subsequently, the results were analyzed by ANOVA (one-way) with *Tukey's* post hoc test, allowing statistically significant differences between curcumin derivatives to be identified ($p < 0.05$).

The molecular docking poses were evaluated for affinity scores and subjected to ANOVA (one-way) with *Tukey's* post hoc test to identify significant differences between curcumin derivatives ($p < 0.05$). In addition, linear regression analysis was performed to investigate the correlation between affinity energy ($E_A$) and pKi values.

### *4.5. Molecular Docking Simulations*

#### 4.5.1. Ligand Preparation and Optimization

The molecular structures of CUR derivatives [23] were illustrated in MarvinSketch Version 23.2.0 [69] (https://www.certara.com/marvin/ accessed on 12 March 2026) and subsequently subjected to structural optimization using the MMFF94 (Merck Molecular Force Field 94) classical force field formalism [70]. The optimization procedures were performed in Avogadro software Version 1.2.0, using the *Steepest Descent* algorithm to minimize the potential energy within the MMFF94 force field model [71].

#### 4.5.2. Obtaining and Preparation of Protein Structures

The structure of glutathione *S*-transferase from shrimp *L. vannamei* (*Lv*GSTmu) was obtained from the Protein Data Bank (http://www.rcsb.org/pdb/home/home.do accessed on 12 March 2026) [72], deposited with the code PDB 5AN1 (Crystal structure of a class-mu glutathione S-transferase from whiteleg shrimp *L. vannamei*: structural changes in the xenobiotic binding H-site may alter the spectra of molecules bound), generated from X-ray diffraction with a resolution of 2.00 Å, classified as a transferase, *E. coli* expression system, *P. vannamei* organism, and complexed with the ligand (glutathione, GSH) [73]. The proteins for the molecular docking were prepared by removing the residues ($H_2O$ and GSH), then adding the polar (H) hydrogens, after which the structure was saved in PDBQT format.

#### 4.5.3. General Docking Procedures

Molecular docking simulations were performed using the AutoDock Vina program Version 1.5.7 [74]. The gridbox was defined to cover the entire *Lv*GSTMu protein, centered at coordinates x = −27.97, y = −8.057, and z = −72.135, with dimensions of 92 Å × 124 Å × 114 Å on the x, y, and z axes, respectively. *Gasteiger* partial charges were assigned to ligands and *Kollman* charges to proteins, with nonpolar hydrogen atoms removed during structure preparation. All other parameters were kept at their default values. The selected conformation was the one that showed the highest binding affinity [75].

Thus, molecular docking simulations were conducted, in which each run generated multiple distinct conformations of the ligand, using an *Exhaustiveness* parameter of 64 [76]. The simulations produced different binding energy values, and the pose associated with the lowest free binding energy was selected as the predominant pose [77]. The stability of the protein-ligand complexes was evaluated based on affinity energy ($E_A$), considering values below −6.0 kcal/mol as indicative of energetically favorable interactions [78].

$$Ki = e^{\left(\frac{\Delta G}{RT}\right)} \quad (7)$$

$$\Delta G = \left(V_{bound}^{L-L} - V_{unbound}^{L-L}\right) + \left(V_{bound}^{P-P} - V_{unbound}^{P-P}\right) + \left(V_{bound}^{P-L} - V_{unbound}^{P-L}\right) + \Delta S_{conf} \quad (8)$$

In addition, the affinity energy and inhibition constant (Ki) were calculated for each protein–ligand complex, according to Equations (7) and (8). In this analysis, Ki represents the inhibition constant, T represents the absolute temperature (298 K), R represents the universal gas constant (8.32 $J{\cdot}mol^{-1}{\cdot}K^{-1}$), and ΔG (adapted in EA) represents the free binding energy ($kJ{\cdot}mol^{-1}$) [79,80].

The term *V* corresponds to the energy contribution of the interactions between the atoms of the ligand (*L*) and the protein (*P*) [81], while $\Delta S_{conf}$ represents the negative conformational entropy change associated with the formation of the L–P complex [82,83].

The methodological and statistical validation of the simulations was conducted using redocking procedures, with evaluation of RMSD (Root Mean Square Deviation) values, adopting 2.0 Å as the reliability criterion [79,82]. All simulations were performed under standardized parameters, ensuring direct comparability of the results obtained for the co-crystallized GSH ligand.

### *4.6. NMA-Model Molecular Dynamics*

The structural dynamics of the target macromolecule (PDB: 5AN1) were investigated using Normal Mode Analysis (NMA) with the iMODS (Internal Coordinates Normal Mode Analysis Server) (https://imods.iqf.csic.es/ accessed on 12 March 2026) web server [84]. This approach allows the exploration of low-frequency collective motions associated with relevant biological functions, such as conformational transitions, intrinsic flexibility, and structural rearrangements [85].

Initially, the prepared structure was submitted to the iMODS server, which performs NMA using internal coordinates, especially dihedral angles, instead of Cartesian coordinates. This strategy reduces computational cost and preserves the stereochemistry of the macromolecule, making the method more suitable for large biological systems [86].

The iMODS algorithm constructs a Hessian matrix based on simplified harmonic potentials and calculates the normal modes of vibration, with special attention to low-frequency modes, which represent collective and biologically relevant movements. These modes describe energetically favorable structural deformations around an equilibrium conformation [86].

The local flexibility of the macromolecule was evaluated using the deformability profile, which indicates regions that are structurally more susceptible to movement. In addition, the theoretical B-factor, derived from normal modes, was analyzed, allowing qualitative comparison with experimental crystallography data when available [87].

In summary, collective movements were visualized through animations of normal modes provided by the server, allowing the identification of regions that move in a concerted manner [88]. Furthermore, the cross-correlation matrix was used to evaluate the positive or negative correlation between the displacements of different residues, helping to understand the internal structural communication of the macromolecule [89].

In addition, analysis of conformational transition trajectories (morphing) between two distinct structures of the same macromolecule, such as active and inactive states, was employed [89]. These trajectories provide a qualitative view of energetically accessible conformational paths, contributing to the understanding of functional mechanisms [86].

## 5. Conclusions

This study integrated molecular modeling, redox property prediction, and ecotoxicological assessment to investigate the biotechnological potential of curcumin derivatives in *L. vannamei*. Docking analyses indicated stable interactions between the compounds and the *Lv*GSTmu enzyme, which is involved in the antioxidant response. Molecular dynamics simulations elucidated the conformational stability of the complexes, with the CURNO derivative promoting a relevant stabilizing effect in the binding cavity without inducing global structural changes in the protein, which may enable its plausibility as a redox modulator.

From an environmental point of view, most derivatives showed low bioaccumulation potential and moderate persistence, although CURH and CURNO showed a greater tendency to remain in sediments. Toxicity varied between trophic levels and exposure times, with greater sensitivity of invertebrates in the acute scenario and fish in chronic exposure, but without statistically significant differences in overall toxicity between the derivatives and curcumin.

Limitations include the predictive nature of in silico approaches and the lack of direct experimental validation in aquatic organisms. In the future, in vivo trials and biochemical analyses of antioxidant markers will be essential to confirm the functional potential of these compounds. Nevertheless, the results position CURNO as a promising candidate, combining molecular affinity, dynamic stability, and an acceptable ecotoxicological profile, although its environmental behavior indicates the need for additional monitoring.

**Supplementary Materials:** The following supporting information can be downloaded at: https://www.mdpi.com/article/10.3390/ddc5020024/s1, Table S1: Ecotoxicity of CUR-derivatives in aquatic organisms.

**Author Contributions:** Conceptualization, D.S.d.S. and J.M.L.d.M.L.; methodology, D.S.d.S. and E.S.M.; investigation, J.M.L.d.M.L., C.S.B.S.-V. and D.S.d.S.; funding acquisition, C.S.B.S.-V. and E.S.M.; writing—original draft preparation, D.S.d.S., J.M.L.d.M.L. and C.S.B.S.-V.; writing—review and editing, C.S.B.S.-V. and E.S.M. All authors have read and agreed to the published version of the manuscript.

**Funding:** Emmanuel Silva Marinho acknowledges financial support from the Funding Agency of Ceará—FUNCAP [Grant: FPD-0213-00369.01.00/23], the National Council for Scientific and Technological Development CNPQ-PQ [Grant: 309349/2025-7], CNPQ-UNIVERSAL [Grant: 407457/2025-9], and the Funding Agency of Ceará—FUNCAP [Grant: COGEFIT 09566252/2022].

**Institutional Review Board Statement:** Not applicable.

**Informed Consent Statement:** Not applicable.

**Data Availability Statement:** The datasets generated and/or analyzed during the current study are available from the corresponding author upon request.

**Acknowledgments:** The authors also thank the Conselho Nacional de Desenvolvimento Científico e Tecnológico (CNPq) and Coordenação de Aperfeiçoamento de Pessoal de Nível Superior (CAPES).

**Conflicts of Interest:** The authors declare no conflicts of interest.

## Abbreviations

The following abbreviations are used in this manuscript:

| | |
|---|---|
| WSSV | White Spot Syndrome Virus |
| QSAR | Quantitative Structure–Activity Relationship |
| MMFF94 | Merck Molecular Force Field 94 |
| *Lv*GSTmu | Glutathione *S*-Transferase from shrimp *L. vannamei* |
| PDB | Protein Data Bank |
| NOS | Nitric oxide scavenger |
| ROS | Reactive oxygen species |
| GST | Glutathione S-Transferase |
| GSH | Glutathione (co-crystallized) |
| CUR | Curcumin |
| NMA | Normal Mode Analysis |
| EA | Affinity energy |
| RMSD | Root Mean Square Deviation |
| ChV | Chronic Toxicity |
| BCF | Bioconcentration factors |
| DM | *Daphnia magna* |
| BAF | Bioaccumulation factors |
| logKow | Octanol-water partition coefficient |
| nP | non-persistent |
| P | Persistent |
| vP | Very persistent |
| NOEC | No observed effect concentrations |
| LOEC | Lowest observed effect concentrations |
| LC50 | Lethal concentration |
| EC50 | Effective concentration |
| NMA | Multilevel Neighborhoods of Atoms |
| PASS | Prediction of Activity Spectra for Substances |
| pKi | Negative logarithm of the inhibition constant |

## Appendix A

**Table A1.** Ligand–receptor (L-R) interaction in the redocking process of the CUR derivatives.

| Compd | Inter. Type | Residues/Distances (Å) |
|---|---|---|
| CURH | Hydrophobic | Y7 (4.70), A12 (4.71), L13 (4.76), K43 (4.12), L60 (3.77), F112 (4.77), F112 (3.38), F112 (3.53), Y116 (3.58), Y116 (4.03), Y116 (3.54), Y116 (3.67), E117 (3.93) |
| | H-bond | Y7 (3.46), W8 (4.06), W46 (1.92), K50 (3.08), L60 (3.96), T113 (3.04), N208 (3.46) |
| | π-Stacking | W8 (5.43) |
| CUROH | Hydrophobic | Y7 (4.64), A12 (4.47), L13 (4.93), L13 (3.93), L60 (3.53), F112 (3.90), F112 (4.17), F112 (3.44), Y116 (3.60), Y116 (4.12), Y210 (4.63) |
| | H-bond | Y7 (2.32), W8 (3.59), K43 (1.82), W46 (2.54), T113 (3.56), T113 (3.68), E117 (3.82), E117 (3.17), Y210 (3.44) |
| | π-Stacking | W8 (4.93), Y116 (3.87) |
| CURBr | Hydrophobic | Y7 (4.94), W8 (4.19), W46 (4.61), L60 (3.36), F112 (3.67), F112 (3.62), Ty116 (4.39), Ty116 (3.70), Ty116 (4.13), Ty116 (3.61) |
| | H-bond | Y7 (2.42), W46 (2.35), K50 (2.36), T113 (2.00) |
| CURCl | Hydrophobic | Y7 (4.20), W8 (3.94), L13 (4.49), W46 (4.77), L60 (3.67), F112 (4.97), F112 (4.54), F112 (3.96), F112 (3.45), Y116 (3.73), Y116 (3.70), Y210 (4.88) |
| | H-bond | Y7 (1.82), W8 (3.41), L13 (3.80), W46 (2.47), K50 (2.44), L60 (3.95), E117 (3.58), E117 (2.81), E117 (4.32), N208 (3.75) |
| | π-Stacking | Y116 (3.99) |
| CURF | Hydrophobic | Y7 (4.39), W8 (4.92), L13 (4.87), L60 (3.82), F112 (4.85), F112 (4.62), F112 (3.65), Y116 (3.63), Y116 (3.65), Y116 (3.74), Y116 (3.93), E117 (4.80) |
| | H-bond | Y7 (1.97), W8 (3.90), W46 (1.99), K50 (2.96), E117 (3.87), E117 (2.23), N208 (3.83) |
| | π-Stacking | W8 (5.35) |
| | Halogen bond | T113 (3.66) |

## References


1. Rameshthangam, P.; Ramasamy, P. Antioxidant and Membrane Bound Enzymes Activity in WSSV-Infected Penaeus Monodon Fabricius. *Aquaculture* **2006**, *254*, 32–39. [CrossRef]
2. Zheng, X.; Yang, J.; Xu, F.; Zhou, Q.; Sun, C.; Wang, A.; Wan, J.; Li, J.; Liu, B. Effect of WSSV Infection on Immunity, Intestinal Microbial Composition and Its Derived Metabolites Synthesis in *Procambarus clarkii*. *Aquac. Rep.* **2025**, *44*, 103055. [CrossRef]
3. Fan, J.; Li, B.; Hong, Q.; Yan, Z.; Yang, X.; Lu, K.; Chen, G.; Wang, L.; Chen, Y. A Glutathione Peroxidase Gene from *Litopenaeus vannamei* Is Involved in Oxidative Stress Responses and Pathogen Infection Resistance. *Int. J. Mol. Sci.* **2022**, *23*, 567. [CrossRef]
4. Valavanidis, A.; Vlahogianni, T.; Dassenakis, M.; Scoullos, M. Molecular Biomarkers of Oxidative Stress in Aquatic Organisms in Relation to Toxic Environmental Pollutants. *Ecotoxicol. Environ. Saf.* **2006**, *64*, 178–189. [CrossRef]
5. Sheehan, D.; Meade, G.; Foley, V.M.; Dowd, C.A. Structure, Function and Evolution of Glutathione Transferases: Implications for Classification of Non-Mammalian Members of an Ancient Enzyme Superfamily. *Biochem. J.* **2001**, *360*, 1–16. [CrossRef]
6. Ma, W.; Zeng, W.; Zhang, D.; Zhou, Y.; Huang, Y.; Hong, Y. Oxidative Stress in Aquaculture: Pathogenic Mechanisms and Preventive Strategies in Farmed Aquatic Animals. *Curr. Issues Mol. Biol.* **2025**, *47*, 873. [CrossRef]
7. Urošević, M.; Nikolić, L.; Gajić, I.; Nikolić, V.; Dinić, A.; Miljković, V. Curcumin: Biological Activities and Modern Pharmaceutical Forms. *Antibiotics* **2022**, *11*, 135. [CrossRef] [PubMed]
8. Musarra-Pizzo, M.; Pennisi, R.; Ben-Amor, I.; Mandalari, G.; Sciortino, M.T. Antiviral Activity Exerted by Natural Products against Human Viruses. *Viruses* **2021**, *13*, 828. [CrossRef] [PubMed]
9. Priyadarsini, K.I. Chemical and Structural Features Influencing the Biological Activity of Curcumin. *Curr. Pharm. Des.* **2013**, *19*, 2093–2100. [CrossRef] [PubMed]
10. He, Y.; Yue, Y.; Zheng, X.; Zhang, K.; Chen, S.; Du, Z. Curcumin, Inflammation, and Chronic Diseases: How Are They Linked? *Molecules* **2015**, *20*, 9183–9213. [CrossRef]
11. Anand, P.; Thomas, S.G.; Kunnumakkara, A.B.; Sundaram, C.; Harikumar, K.B.; Sung, B.; Tharakan, S.T.; Misra, K.; Priyadarsini, I.K.; Rajasekharan, K.N.; et al. Biological Activities of Curcumin and Its Analogues (Congeners) Made by Man and Mother Nature. *Biochem. Pharmacol.* **2008**, *76*, 1590–1611. [CrossRef] [PubMed]
12. Goel, A.; Aggarwal, B.B. Curcumin, the Golden Spice From Indian Saffron, Is a Chemosensitizer and Radiosensitizer for Tumors and Chemoprotector and Radioprotector for Normal Organs. *Nutr. Cancer* **2010**, *62*, 919–930. [CrossRef] [PubMed]
13. Priyadarsini, K.I. The Chemistry of Curcumin: From Extraction to Therapeutic Agent. *Molecules* **2014**, *19*, 20091–20112. [CrossRef] [PubMed]
14. Hewlings, S.J.; Kalman, D.S. Curcumin: A Review of Its Effects on Human Health. *Foods* **2017**, *6*, 92. [CrossRef] [PubMed]
15. Gupta, S.C.; Patchva, S.; Aggarwal, B.B. Therapeutic Roles of Curcumin: Lessons Learned from Clinical Trials. *AAPS J.* **2013**, *15*, 195–218. [CrossRef] [PubMed]
16. Nelson, K.M.; Dahlin, J.L.; Bisson, J.; Graham, J.; Pauli, G.F.; Walters, M.A. The Essential Medicinal Chemistry of Curcumin. *J. Med. Chem.* **2017**, *60*, 1620–1637. [CrossRef]
17. Yallapu, M.M.; Jaggi, M.; Chauhan, S.C. Curcumin Nanoformulations: A Future Nanomedicine for Cancer. *Drug Discov. Today* **2012**, *17*, 71–80. [CrossRef]
18. Kocaadam, B.; Şanlier, N. Curcumin, an Active Component of Turmeric (*Curcuma longa*), and Its Effects on Health. *Crit. Rev. Food Sci. Nutr.* **2017**, *57*, 2889–2895. [CrossRef]
19. Zhao, C.; Liu, Z.; Liang, G. Promising Curcumin-Based Drug Design: Mono-Carbonyl Analogues of Curcumin (MACs). *Curr. Pharm. Des.* **2013**, *19*, 2114–2135. [CrossRef]
20. Khayatan, D.; Razavi, S.M.; Arab, Z.N.; Hosseini, Y.; Niknejad, A.; Momtaz, S.; Abdolghaffari, A.H.; Sathyapalan, T.; Jamialahmadi, T.; Kesharwani, P.; et al. Superoxide Dismutase: A Key Target for the Neuroprotective Effects of Curcumin. *Mol. Cell. Biochem.* **2024**, *479*, 693–705. [CrossRef] [PubMed]
21. Chen, B.; He, Q.; Chen, C.; Lin, Y.; Xiao, J.; Pan, Z.; Li, M.; Li, S.; Yang, J.; Wang, F.; et al. Combination of Curcumin and Catalase Protects against Chondrocyte Injury and Knee Osteoarthritis Progression by Suppressing Oxidative Stress. *Biomed. Pharmacother.* **2023**, *168*, 115751. [CrossRef]
22. Adeseko, C.J.; Fabuyi, F.S. Computational Evaluation of Pharmacokinetics, Potential Bioactive Compounds Targets of Glutathione S-Transferases against Deleterious Effects of MSG: The Health Benefits of Turmeric (*Curcuma longa* L.). *Plant Cell Biotechnol. Mol. Biol.* **2025**, *26*, 111–125. [CrossRef]
23. Yang, H.; Du, Z.; Wang, W.; Song, M.; Sanidad, K.; Sukamtoh, E.; Zheng, J.; Tian, L.; Xiao, H.; Liu, Z.; et al. Structure–Activity Relationship of Curcumin: Role of the Methoxy Group in Anti-Inflammatory and Anticolitis Effects of Curcumin. *J. Agric. Food Chem.* **2017**, *65*, 4509–4515. [CrossRef] [PubMed]
24. Mackay, D.; Fraser, A. Bioaccumulation of Persistent Organic Chemicals: Mechanisms and Models. *Environ. Pollut.* **2000**, *110*, 375–391. [CrossRef] [PubMed]
25. Dearden, J.C. The History and Development of Quantitative Structure-Activity Relationships (QSARs). *Int. J. Quant. Struct.-Prop. Relatsh.* **2016**, *1*, 1–44. [CrossRef]

26. Anand, P.; Kunnumakkara, A.B.; Newman, R.A.; Aggarwal, B.B. Bioavailability of Curcumin: Problems and Promises. *Mol. Pharm.* **2007**, *4*, 807–818. [CrossRef]
27. Arnot, J.A.; Gobas, F.A. A Review of Bioconcentration Factor (BCF) and Bioaccumulation Factor (BAF) Assessments for Organic Chemicals in Aquatic Organisms. *Environ. Rev.* **2006**, *14*, 257–297. [CrossRef]
28. Sanderson, H. Probabilistic Hazard Assessment of Environmentally Occurring Pharmaceuticals Toxicity to Fish, Daphnids and Algae by ECOSAR Screening. *Toxicol. Lett.* **2003**, *144*, 383–395. [CrossRef] [PubMed]
29. Arnot, J.A.; Meylan, W.; Tunkel, J.; Howard, P.H.; Mackay, D.; Bonnell, M.; Boethling, R.S. A Quantitative Structure-Activity Relationship for Predicting Metabolic Biotransformation Rates for Organic Chemicals in Fish. *Environ. Toxicol. Chem.* **2009**, *28*, 1168–1177. [CrossRef]
30. Arnot, J.A.; Gobas, F.A.P.C. A Generic QSAR for Assessing the Bioaccumulation Potential of Organic Chemicals in Aquatic Food Webs. *QSAR Comb. Sci.* **2003**, *22*, 337–345. [CrossRef]
31. Kelly, B.C.; Sun, J.M.; McDougall, M.R.R.; Sunderland, E.M.; Gobas, F.A.P.C. Development and Evaluation of Aquatic and Terrestrial Food Web Bioaccumulation Models for Per- and Polyfluoroalkyl Substances. *Environ. Sci. Technol.* **2024**, *58*, 17828–17837. [CrossRef] [PubMed]
32. Arnot, J.A.; Toose, L.; Armitage, J.M.; Embry, M.; Sangion, A.; Hughes, L. A Weight of Evidence Approach for Bioaccumulation Assessment. *Integr. Environ. Assess. Manag.* **2023**, *19*, 1235–1253. [CrossRef] [PubMed]
33. Rand, G.M. (Ed.) *Fundamentals of Aquatic Toxicology: Effects, Environmental Fate, and Risk Assessment*, 2nd ed.; CRC Press: Boca Raton, FL, USA, 2020; ISBN 978-1-003-07536-3.
34. Ghorpade-Aher, J.; Saxena, A.; Inamdar, M.; Thakre, A.; Sinha, D.; Thesiya, T. QSAR Model for Aquatic Toxicity Estimates Using Machine Learning. In *Advances in Communication and Applications*; Patnaik, L.M., Ravikumar, G.K., Prasad, N.H., Eds.; Lecture Notes in Electrical Engineering; Springer Nature: Singapore, 2025; Volume 1398, pp. 387–398. ISBN 978-981-96-4678-4.
35. Pizzo, F.; Lombardo, A.; Brandt, M.; Manganaro, A.; Benfenati, E. A New Integrated in Silico Strategy for the Assessment and Prioritization of Persistence of Chemicals under REACH. *Environ. Int.* **2016**, *88*, 250–260. [CrossRef]
36. Moghadam, H.; Sourinejad, I.; Johari, S.A. Dietary Turmeric, Curcumin and Nanoencapsulated Curcumin Can Differently Fight against Salinity Stress in Pacific White Shrimp Penaeus Vannamei Boone, 1931. *Aquac. Res.* **2022**, *53*, 3127–3139. [CrossRef]
37. Song, L.; Li, M.; Feng, C.; Sa, R.; Hu, X.; Wang, J.; Yin, X.; Qi, C.; Dong, W.; Yang, J. Protective Effect of Curcumin on Zebrafish Liver under Ethanol-Induced Oxidative Stress. *Comp. Biochem. Physiol. Part C Toxicol. Pharmacol.* **2022**, *258*, 109360. [CrossRef]
38. Tuong, D.T.C.; Moniruzzaman, M.; Smirnova, E.; Chin, S.; Sureshbabu, A.; Karthikeyan, A.; Min, T. Curcumin as a Potential Antioxidant in Stress Regulation of Terrestrial, Avian, and Aquatic Animals: A Review. *Antioxidants* **2023**, *12*, 1700. [CrossRef]
39. Tugcu, G.; Sipahi, H.; Charehsaz, M.; Aydın, A.; Saçan, M.T. Computational Toxicology of Pharmaceuticals. In *Cheminformatics, QSAR and Machine Learning Applications for Novel Drug Development*; Elsevier: Amsterdam, The Netherlands, 2023; pp. 519–537. ISBN 978-0-443-18638-7.
40. Gao, J.; Zhao, J.; Chen, X.; Wang, J. A Review on in Silico Prediction of the Environmental Risks Posed by Pharmaceutical Emerging Contaminants. *Environ. Monit. Assess.* **2023**, *195*, 1535. [CrossRef]
41. Grillo-Avila, D.; Antón-Pardo, M.; Armengol, J.; Puche, E.; Carballeira, R.; Moratalla-López, J.; Palacios-Abella, J.F.; López, I.; Crettaz Minaglia, M.C.; Amador, P.; et al. Effects of the Herbicide Bentazone on the Structure of Plankton and Benthic Communities Representative of Mediterranean Coastal Wetlands: A Mesocosm Experiment. *Hydrobiologia* **2025**, *852*, 2709–2728. [CrossRef]
42. Tkaczyk, A.; Bownik, A.; Dudka, J.; Kowal, K.; Ślaska, B. Daphnia Magna Model in the Toxicity Assessment of Pharmaceuticals: A Review. *Sci. Total Environ.* **2021**, *763*, 143038. [CrossRef]
43. Glowienke, S.; Onken, U.; Elhajouji, A.; Muthusamy, S.; Sangana, R.; Martus, H.-J.; Bedman, T.; Hartmann, A. Genotoxicity Evaluation of a Valsartan-Related Complex N-Nitroso-Impurity. *Regul. Toxicol. Pharmacol.* **2022**, *134*, 105245. [CrossRef] [PubMed]
44. Han, J.; Yang, D.; Hall, D.R.; Liu, J.; Sun, J.; Gu, W.; Tang, S.; Alharbi, H.A.; Jones, P.D.; Krause, H.M.; et al. Toxicokinetics of Brominated Azo Dyes in the Early Life Stages of Zebrafish (*Danio rerio*) Is Prone to Aromatic Substituent Changes. *Environ. Sci. Technol.* **2020**, *54*, 4421–4431. [CrossRef]
45. Salvatore, M.M.; Pappalardo, C.; Suarez, E.G.P.; Salvatore, F.; Andolfi, A.; Gesuele, R.; Galdiero, E.; Libralato, G.; Guida, M.; Siciliano, A. Ecotoxicological and Metabolomic Investigation of Chronic Exposure of *Daphnia magna* (Straus, 1820) to Yttrium Environmental Concentrations. *Aquat. Toxicol.* **2024**, *276*, 107117. [CrossRef]
46. Zhu, J.; Huang, M.; Liu, C.; Wang, J.; Zou, L.; Yang, F.; Zhu, R. Curcumin Protects against Fenvalerate-Induced Neurotoxicity in Zebrafish (*Danio rerio*) Larvae through Inhibition of Oxidative Stress. *Ecotoxicol. Environ. Saf.* **2023**, *264*, 115484. [CrossRef]
47. Boya, B.R.; Lee, J.-H.; Choi, J.-M.; Lee, J. Impact of Halogenation on Scaffold Toxicity Assessed Using HD-GEM Machine Learning Model. *Brief. Bioinform.* **2025**, *26*, bbaf347. [CrossRef]
48. Jayaprakasha, G.K.; Jaganmohan Rao, L.; Sakariah, K.K. Antioxidant Activities of Curcumin, Demethoxycurcumin and Bisdemethoxycurcumin. *Food Chem.* **2006**, *98*, 720–724. [CrossRef]
49. Falade, V.A.; Adelusi, T.I.; Adedotun, I.O.; Abdul-Hammed, M.; Lawal, T.A.; Agboluaje, S.A. In Silico Investigation of Saponins and Tannins as Potential Inhibitors of SARS-CoV-2 Main Protease ($M^{pro}$). *In Silico Pharmacol.* **2021**, *9*, 9. [CrossRef] [PubMed]

50. Al-Zaqri, N.; Pooventhiran, T.; Rao, D.J.; Alsalme, A.; Warad, I.; Thomas, R. Structure, Conformational Dynamics, Quantum Mechanical Studies and Potential Biological Activity Analysis of Multiple Sclerosis Medicine Ozanimod. *J. Mol. Struct.* **2021**, *1227*, 129685. [CrossRef]
51. Lagunin, A.; Stepanchikova, A.; Filimonov, D.; Poroikov, V. PASS: Prediction of Activity Spectra for Biologically Active Substances. *Bioinformatics* **2000**, *16*, 747–748. [CrossRef]
52. Filimonov, D.A.; Lagunin, A.A.; Gloriozova, T.A.; Rudik, A.V.; Druzhilovskii, D.S.; Pogodin, P.V.; Poroikov, V.V. Prediction of the Biological Activity Spectra of Organic Compounds Using the Pass Online Web Resource. *Chem. Heterocycl. Comp.* **2014**, *50*, 444–457. [CrossRef]
53. Hansch, C. Quantitative Structure-Activity Relationships and the Unnamed Science. *Acc. Chem. Res.* **1993**, *26*, 147–153. [CrossRef]
54. Filimonov, D.; Poroikov, V.; Borodina, Y.; Gloriozova, T. Chemical Similarity Assessment through Multilevel Neighborhoods of Atoms: Definition and Comparison with the Other Descriptors. *J. Chem. Inf. Comput. Sci.* **1999**, *39*, 666–670. [CrossRef]
55. Filimonov, D.A.; Zakharov, A.V.; Lagunin, A.A.; Poroikov, V.V. QNA-Based 'Star Track' QSAR Approach. *SAR QSAR Environ. Res.* **2009**, *20*, 679–709. [CrossRef]
56. Pereira, A.C.M.; Sánchez-Ortíz, B.L.; de Melo, E.L.; da Silva Hage-Melim, L.I.; Borges, R.S.; Hu, X.; Carvalho, J.C.T. Perillyl Alcohol Decreases the Frequency and Severity of Convulsive-like Behavior in the Adult Zebrafish Model of Acute Seizures. *Naunyn-Schmiedeberg's Arch. Pharmacol.* **2021**, *394*, 1177–1190. [CrossRef]
57. Furuhama, A.; Hasunuma, K.; Aoki, Y. Interspecies Quantitative Structure–Activity Relationships (QSARs) for Eco-Toxicity Screening of Chemicals: The Role of Physicochemical Properties. *SAR QSAR Environ. Res.* **2015**, *26*, 809–830. [CrossRef]
58. U.S. Environmental Protection Agency. Ecological Structure—Activity Relationships Program (ECOSAR) Operation Manual v2.2. Available online: https://www.epa.gov/tsca-screening-tools/ecological-structure-activity-relationships-program-ecosar-operation-manual (accessed on 13 March 2026).
59. Netzeva, T.I.; Pavan, M.; Worth, A.P. Review of (Quantitative) Structure–Activity Relationships for Acute Aquatic Toxicity. *QSAR Comb. Sci.* **2008**, *27*, 77–90. [CrossRef]
60. Comber, M.H.I.; Walker, J.D.; Watts, C.; Hermens, J. Quantitative Structure-activity Relationships for Predicting Potential Ecological Hazard of Organic Chemicals for Use in Regulatory Risk Assessments. *Environ. Toxicol. Chem.* **2003**, *22*, 1822–1828. [CrossRef] [PubMed]
61. de Sousa, D.S.; Gomes, A.O.C.V.; Roberto, C.H.A.; Belarmino, A.B.; da Silva Mendes, F.R.; Marinho, M.M.; de Lima-Neto, P.; Marinho, G.S. Ligand and Structure-Based Toxicological Assessment of (Thio)Semicarbazones on Cholinesterases. *J. Comput. Aided Mol. Des.* **2026**, *40*, 40. [CrossRef] [PubMed]
62. Kamerlin, N.; Delcey, M.G.; Manzetti, S.; van der Spoel, D. Toward a Computational Ecotoxicity Assay. *J. Chem. Inf. Model.* **2020**, *60*, 3792–3803. [CrossRef]
63. de Sousa, D.S.; de Oliveira, V.M.; Gomes, A.O.C.V.; da Silva Mendes, F.R.; Marinho, M.M.; de Lima-Neto, P.; Marinho, G.S. Computational Investigation of Behavioral Toxicity Syndromes (BTS) of Synthetics Halosubstituted Semicarbazones. *In Silico Pharmacol.* **2025**, *13*, 152. [CrossRef]
64. Roveri, V.; Guimarães, L.L.; Toma, W.; Correia, A.T. Occurrence and Ecological Risk Assessment of Pharmaceuticals and Cocaine in a Beach Area of Guarujá, São Paulo State, Brazil, under the Influence of Urban Surface Runoff. *Environ. Sci. Pollut. Res.* **2020**, *27*, 45063–45075. [CrossRef] [PubMed]
65. Finizio, A.; Di Nica, V.; Rizzi, C.; Villa, S. A Quantitative Structure-Activity Relationships Approach to Predict the Toxicity of Narcotic Compounds to Aquatic Communities. *Ecotoxicol. Environ. Saf.* **2020**, *190*, 110068. [CrossRef]
66. Reuschenbach, P.; Silvani, M.; Dammann, M.; Warnecke, D.; Knacker, T. ECOSAR Model Performance with a Large Test Set of Industrial Chemicals. *Chemosphere* **2008**, *71*, 1986–1995. [CrossRef]
67. Rogiers, V.; Benfenati, E.; Bernauer, U.; Bodin, L.; Carmichael, P.; Chaudhry, Q.; Coenraads, P.J.; Cronin, M.T.D.; Dent, M.; Dusinska, M.; et al. The Way Forward for Assessing the Human Health Safety of Cosmetics in the EU—Workshop Proceedings. *Toxicology* **2020**, *436*, 152421. [CrossRef] [PubMed]
68. Roncaglioni, A.; Lombardo, A.; Benfenati, E. The VEGAHUB Platform: The Philosophy and the Tools. *Altern. Lab. Anim.* **2022**, *50*, 121–135. [CrossRef]
69. Laxmi, K. Characterization of Ligand N′-[(1E)-1-Phenylethylidene]-1,3-Benzothiazole-2-Carbohydrazide by Using Marvin Sketch 20.8 Software. *Orient. J. Chem.* **2022**, *38*, 77–84. [CrossRef]
70. Cheng, A.; Best, S.A.; Merz, K.M.; Reynolds, C.H. GB/SA Water Model for the Merck Molecular Force Field (MMFF). *J. Mol. Graph. Model.* **2000**, *18*, 273–282. [CrossRef]
71. Snyder, H.D.; Kucukkal, T.G. Computational Chemistry Activities with Avogadro and ORCA. *J. Chem. Educ.* **2021**, *98*, 1335–1341. [CrossRef]
72. Goodsell, D.S.; Zardecki, C.; Di Costanzo, L.; Duarte, J.M.; Hudson, B.P.; Persikova, I.; Segura, J.; Shao, C.; Voigt, M.; Westbrook, J.D.; et al. RCSB Protein Data Bank: Enabling Biomedical Research and Drug Discovery. *Protein Sci.* **2020**, *29*, 52–65. [CrossRef] [PubMed]

73. Juárez-Martínez, A.B.; Sotelo-Mundo, R.R.; Rudiño-Piñera, E. Crystal Structure of a Class-Mu Glutathione S-Transferase from Whiteleg Shrimp *Litopenaeus vannamei*: Structural Changes in the Xenobiotic Binding H-Site May Alter the Spectra of Molecules Bound. *J. Biochem. Mol. Toxicol.* **2017**, *31*, e21838. [CrossRef]
74. De Sousa, D.S.; Moreira de Oliveira, V.; Silva Marinho, E.; Sandra Brito Salmito-Vanderley, C.; Silva Marinho, G. Insights of Potential Action with Acyclovir Analogs for the Control of White Spot Syndrome Virus (WSSV): Molecular Dynamics and Ecotoxicological Analysis Approach. *Microb. Pathog.* **2025**, *208*, 107955. [CrossRef]
75. de Oliveira, V.M.; da Rocha, M.N.; Roberto, C.H.A.; Lucio, F.N.M.; Marinho, M.M.; Marinho, E.S.; de Morais, S.M. Insights of Structure-Based Virtual Screening and MPO-Based SAR Analysis of Berberine-Benzimidazole Derivatives against Parkinson Disease. *J. Mol. Struct.* **2024**, *1302*, 137453. [CrossRef]
76. Callil-Soares, P.H.; Biasi, L.C.K.; Pessoa Filho, P.D.A. Effect of Preprocessing and Simulation Parameters on the Performance of Molecular Docking Studies. *J. Mol. Model.* **2023**, *29*, 251. [CrossRef]
77. Silva, J.; Esmeraldo Rocha, J.; da Cunha Xavier, J.; Sampaio de Freitas, T.; Douglas Melo Coutinho, H.; Nogueira Bandeira, P.; Rodrigues de Oliveira, M.; Nunes da Rocha, M.; Machado Marinho, E.; de Kassio Vieira Monteiro, N.; et al. Antibacterial and Antibiotic Modifying Activity of Chalcone (2E)-1-(4′-Aminophenyl)-3-(4-Methoxyphenyl)-Prop-2-En-1-One in Strains of Staphylococcus Aureus Carrying NorA and MepA Efflux Pumps: In Vitro and in Silico Approaches. *Microb. Pathog.* **2022**, *169*, 105664. [CrossRef]
78. Belarmino, A.B.; de Sousa, D.S.; Henrique Alexandre Roberto, C.; Moreira de Oliveira, V.; Nunes da Rocha, M.; Rogenio da Silva Mendes, F.; Machado Marinho, M.; Marques da Fonseca, A.; Silva Marinho, G. Ligand-Based Analysis of the Antifungal Potential of Phytosterols and Triterpenes Isolated from Cryptostegia Grandiflora against *Candida auris* FKBP12. *Steroids* **2024**, *209*, 109453. [CrossRef]
79. Morris, G.M.; Huey, R.; Lindstrom, W.; Sanner, M.F.; Belew, R.K.; Goodsell, D.S.; Olson, A.J. AutoDock4 and AutoDockTools4: Automated Docking with Selective Receptor Flexibility. *J. Comput. Chem.* **2009**, *30*, 2785–2791. [CrossRef] [PubMed]
80. Morris, G.M.; Goodsell, D.S.; Halliday, R.S.; Huey, R.; Hart, W.E.; Belew, R.K.; Olson, A.J. Automated Docking Using a Lamarckian Genetic Algorithm and an Empirical Binding Free Energy Function. *J. Comput. Chem.* **1998**, *19*, 1639–1662. [CrossRef]
81. Shityakov, S.; Förster, C. In Silico Predictive Model to Determine Vector-Mediated Transport Properties for the Blood–Brain Barrier Choline Transporter. *Adv. Appl. Bioinform. Chem.* **2014**, *7*, 23–36. [CrossRef] [PubMed]
82. Yusuf, D.; Davis, A.M.; Kleywegt, G.J.; Schmitt, S. An Alternative Method for the Evaluation of Docking Performance: RSR vs RMSD. *J. Chem. Inf. Model.* **2008**, *48*, 1411–1422. [CrossRef]
83. Morris, G.M.; Huey, R.; Olson, A.J. Using AutoDock for Ligand-Receptor Docking. *Curr. Protoc. Bioinform.* **2008**, *24*, 8.14.1–8.14.40. [CrossRef] [PubMed]
84. da Rocha, M.N.; da Fonseca, A.M.; Dantas, A.N.M.; dos Santos, H.S.; Marinho, E.S.; Marinho, G.S. In Silico Study in MPO and Molecular Docking of the Synthetic Drynaran Analogues Against the Chronic Tinnitus: Modulation of the M1 Muscarinic Acetylcholine Receptor. *Mol. Biotechnol.* **2024**, *66*, 254–269. [CrossRef]
85. do Nascimento Gonçalves, C.; da Rocha, M.N.; Marinho, E.S. In Silico Identification of Benzamide-Based Aryl Halides as EGFR Inhibitors: Multi-Ligand ADMET, Pharmacophore Mapping, and Target Prediction. *In Silico Res. Biomed.* **2026**, *2*, 100164. [CrossRef]
86. Lopéz-Blanco, J.R.; Garzón, J.I.; Chacón, P. iMod: Multipurpose Normal Mode Analysis in Internal Coordinates. *Bioinformatics* **2011**, *27*, 2843–2850. [CrossRef] [PubMed]
87. Kovacs, J.A.; Chacón, P.; Abagyan, R. Predictions of Protein Flexibility: First-Order Measures. *Proteins Struct. Funct. Bioinform.* **2004**, *56*, 661–668. [CrossRef] [PubMed]
88. Pinheiro, N.A.P.; Romão, I.C.; Alves, A.M.B.; Siqueira, S.M.C.; de Menezes, J.E.S.A.; Marinho, E.S.; Ferreira, M.K.A.; Marinho, M.M.; de Sousa Magalhães, H.; de Castro Gomes, A.F.; et al. Serotonergic Neuromodulation of Natural Products Isoreserpine and Isoreserpiline in Adult Zebrafish: An in Silico and In Vivo Investigation. *Chem. Biodivers.* **2026**, *23*, e01738. [CrossRef] [PubMed]
89. López-Blanco, J.R.; Aliaga, J.I.; Quintana-Ortí, E.S.; Chacón, P. iMODS: Internal Coordinates Normal Mode Analysis Server. *Nucleic Acids Res.* **2014**, *42*, W271–W276. [CrossRef] [PubMed]